

Identifying source and evaluation of hydrogeochemical processes in the hard rock aquifer system: geostatistical analysis and geochemical modeling techniques

N. Janardhana Raju¹ · Priyanka Patel¹ · B. C. Sundara Raja Reddy² · U. Suresh² · T. V. K. Reddy²

Received: 17 February 2016 / Accepted: 3 August 2016 / Published online: 10 August 2016
© Springer-Verlag Berlin Heidelberg 2016

Abstract In order to quantify spatio-temporal changes in the hydrogeochemistry of Swarnamukhi river basin, Andhra Pradesh, India, a total of 239 groundwater samples have been collected for pre- and post-monsoon seasons of 2014 and 2015. The geology of the study area is comprised of granite, granitic gneisses, shales, quartzites, laterites and recent alluvium along the river course. Based on the study of geochemical processes of different seasons, it is found that the occurrence of Na and HCO₃ in 2014 shifted toward Ca and HCO₃ in 2015 due to cation exchange process. Fe shows the higher concentration value than safe limit due to dissolution of ferruginous minerals and domestic sewage discharges. Bivariate plots of various ions and ratios depict the predominance of silicate weathering over carbonate and evaporite dissolution apart from anthropogenic activities in the enrichment of groundwater constituents. High nitrate concentration was observed in the urbanized regions of the basin followed by intense agricultural areas. Geochemical modeling was carried out using mineral saturation index and thermodynamic stability plots to deduce major weathered products. Most of the groundwater samples in the study area are saturated with carbonate minerals but are undersaturated with silicate minerals. Thermodynamic stability plots suggest the formation of kaolinite secondary mineral and presence of aluminosilicate minerals. Fuzzy calculation is applied to determine the water quality index, which categorizes a majority of the samples as excellent to

good category for human use. Factor analysis points toward the mixed source identification of ionic constituents. Saline water mixing index model calculation suggests the effect of salinization in coastal areas due to heavy withdrawal of the fresh groundwater resources for various uses, whereas in the mainland it is due to agricultural runoff and domestic waste water.

Keywords Hydrogeochemical processes · Water quality index · Geochemical modeling · Statistical techniques · Saline water intrusion

Introduction

Water is an important, infinite and expendable natural resource which forms a center of ecological system via hydrological cycle. According to Shiklomanov (1993), 96.5 % ($1338 \times 10^6 \text{ km}^3$) of the world's water is in oceans, but high salinity renders the oceans virtually unusable for humans. The remainder is distributed in glaciers (1.74 % or $24.1 \times 10^6 \text{ km}^3$), groundwater (1.70 % or $23.4 \times 10^6 \text{ km}^3$), permafrost, lakes, rivers and atmospheric water as a freshwater stock. Groundwater is considered safe from pathogens and other chemical contaminants due to natural infiltration capacity of aquifer material and, thus, necessitates a little infection. So, the groundwater has become an appropriate alternative over surface freshwater reservoirs for different purposes, such as drinking, irrigation and various industrial processes (Raju and Reddy 1998; Nampak et al. 2014; Singh et al. 2015). Geochemical behavior of groundwater becomes altered in due course of time while circulating in the hydrological cycle and streaming from recharge to discharge areas through factors such as rock weathering, aquifer lithology, evaporation,

✉ Priyanka Patel
prirocks11@gmail.com

¹ School of Environmental Sciences, Jawaharlal Nehru University, New Delhi 110067, India

² Department of Geology, S.V. University, Tirupati, Andhra Pradesh 517502, India

cation exchange, quality of recharge water, selective uptake by vegetation, atmospheric precipitation, leaching of fertilizers, industrialization and urbanization (Raju and Reddy 2007). So, an understanding of its characterization and exploration is helpful in groundwater sustainable management and quality (Raju et al. 1996, 2012; Reddy et al. 2000; Ayenew et al. 2008; Rao et al. 2013; Zouahri et al. 2014).

Coastal aquifers, particularly of semiarid and arid regions, are susceptible to salinization due to seawater intrusion, wastewater recycling, overextraction of groundwater from coastal areas, up-coning of paleobrine bodies near to fresh groundwater bodies, aquifer geology and irrigation return flow (Cendón et al. 2008; Einsiedl 2012). Various geochemical, hydrodynamic and numerical modeling techniques are established for predicting the salinization phenomenon (Reddy et al. 1992; Mondal et al. 2011; Zghibi et al. 2014). Geochemical studies are characterized by large amounts of data with high heterogeneity due to various natural and anthropogenic factors; thus, application of multivariate statistical methods avoids the misinterpretation of data, unveils the hidden information about spatio-temporal variations and assembles them into statistically distinct hydrochemical groups according to hydrogeological and agricultural context which could be further utilized for scheming of a monitoring network for the efficient water management (Raju et al. 2013; Svetlana et al. 2012; Herojeet et al. 2013; Jung et al. 2014; Machiwal and Jha 2015). Attempts were made for source identification and evaluation of hydrogeochemical processes using geochemical and geostatistical modeling techniques to assess the effect of natural and anthropogenic activities in the Swarnamukhi river basin, Andhra Pradesh, India.

Study area

The study area is comprised of two districts of Andhra Pradesh (Chittoor and Nellore) which covers the whole stretch of Swarnamukhi river (latitudes 13°25'30"N and 14°08'30"N and longitudes 79°07'39"E and 80°11'0"E) (Fig. 1). Population density of the study area is approximately 251 persons/km². Chittoor district of the study area is a highly urbanized center present in mainland, whereas Nellore district is comprised of coastal regions nearer to Bay of Bengal where the river joins the sea. Rainfall in the district is spread across the months of June to September (SW monsoon) and October to December (NE monsoon). The Swarnamukhi is an ephemeral east flowing river which has drainage of 3225 km² and length of about 192 km with dendritic to subdendritic type of drainage pattern. Annual average rainfall of the study area is around 934 mm. The

maximum and minimum temperature in the basin is 46 and 12 °C, respectively.

The Swarnamukhi river basin is underlain by the formations of Archean, Proterozoic and Quaternary ages. Geology of the study area is comprised of granite and granitic gneisses followed by shales, quartzites, laterites and recent alluvium along the river course (Fig. 2). The major portion of the study area is covered by granites and granitic gneisses rocks (~60 %) which are intercepted by innumerable dolerite dyke rocks of narrow width and considerable linear extent. The Dharwar consists of schistose gneisses and is found in a small portion in the lower part of the basin. In the upper part of the river basin, the Archean formations are overlaid by the Precambrian group of Cuddapah formations (quartzites and intercalated shales) which are separated by the Eparchean unconformity. The Cuddapah formation consists of quartzites, shales and phyllites. Laterites are found as a narrow north–south belt running in between the coastal alluvium and the older rocks in the interior. Recent and subrecent formations like old and new alluvium are present along the river courses in the basin. Extensive alluvium deposits along the Swarnamukhi river course form fluvial origin, whereas areas near to Bay of Bengal form coastal origin. Groundwater occurs under unconfined conditions in weathered portion and semiconfined condition in fractures and joints at deeper depths.

Methodology

Groundwater sampling procedure

Physiographic location map has been drawn with the help of toposheets (57O/6, 57O/9, 57O/10, 57O/13, 66B/4 and 66C/1) and Arc GIS 9.3. To understand the spatio-temporal variation, representative samples were uniformly collected from the basin area for 2 years, 2014 and 2015 [$N = 59$ in pre-monsoon 2014 (May 2014), $N = 66$ in post-monsoon 2014 (January 2014), $N = 57$ in pre-monsoon (June 2015) and $N = 57$ in post-monsoon season of 2015 (February 2015)].

Analytical procedure and data treatment

The pH, EC and TDS were measured in the field with a multiparameter ion meter (pH/Cond 340i SET 1). Various physico-chemical parameters and heavy metals were analyzed by the prescribed standard methods (APHA 2005). The analytical precision for measured ions was within ± 5 %, derived by electrical neutrality. Spatial distribution diagram of various parameters was plotted using Arc GIS 9.3 with IDW interpolation technique.

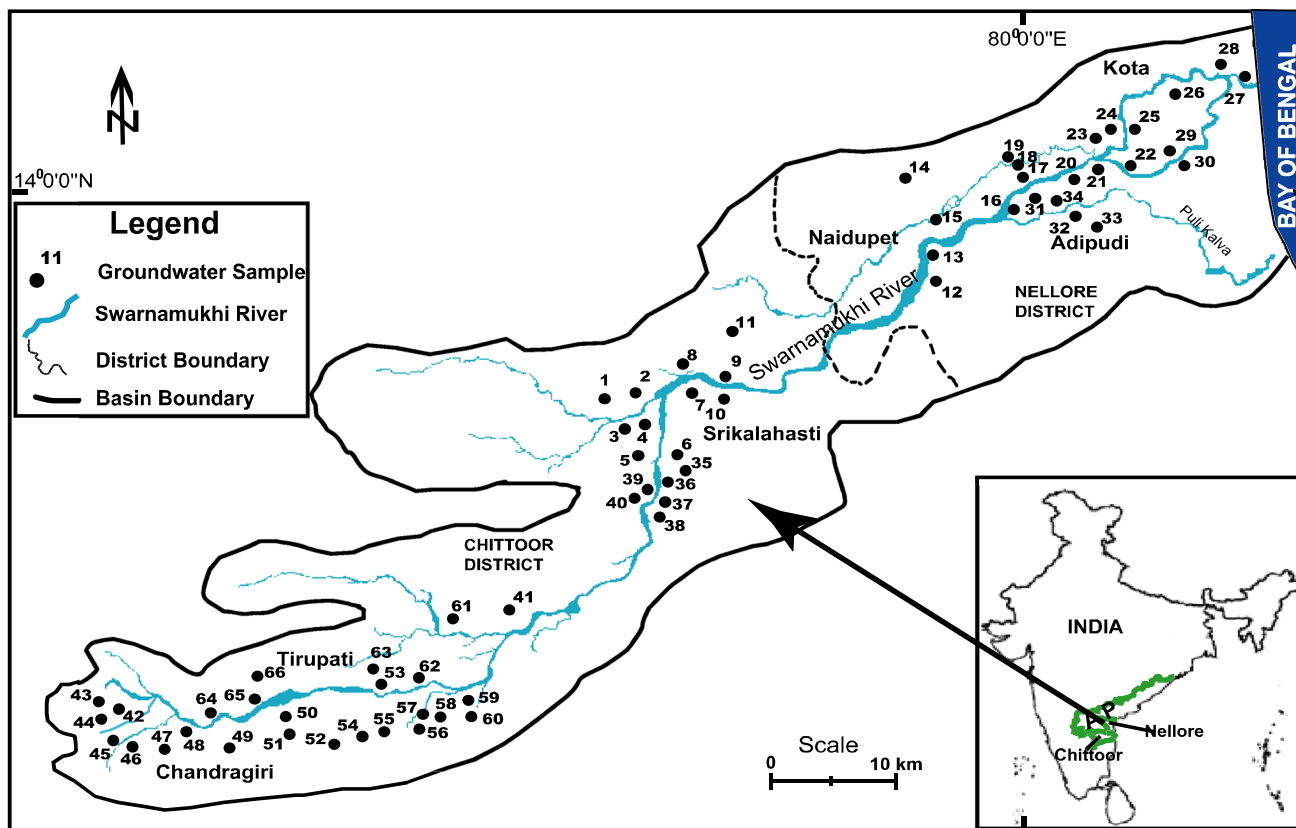


Fig. 1 Physiographic and location map of Swarnamukhi river basin, Andhra Pradesh

Geochemical modeling is helpful to simulate and predict the geochemical reactions. The geochemical equilibrium condition of minerals is evaluated by mathematical and graphical approach. In mathematical approach, saturation index of minerals provides information on equilibrium state attainment between rock matrix and groundwater (Njitchoua et al. 1997), whereas graphical evaluation is through mineral stability fields of ionic activity ratios (Helgeson 1968). $SI < 0$ directs mineral undersaturated state due to dissolution, insufficient amount of mineral for solution or short residence time. $SI = 0$ indicates equilibrium between mineral and groundwater. $SI > 0$ suggests mineral supersaturated condition due to incongruent dissolution or common ion effect (Rasouli et al. 2012; Okiongbo and Douglas 2014). Different saturation indices of minerals were calculated with WATEQ4F program (Ball and Nordstrom 1991).

Hydrochemical results are statistically analyzed by the software IBM SPSS 19 in order to understand geochemical processes occurring in the groundwater of the Swarnamukhi river basin. Varimax rotation with Kaiser normalization method was applied to deduce the factors from the present bulk of analytical data, whereas squared Euclidean distance and ward’s method were applied in hierarchical cluster analysis.

Fuzzy calculation is a useful mathematical tool to rule out inaccuracies and understand water quality with respect to prescribed standards (Zhang et al. 2012; Kumar et al. 2014). The linear fuzzy membership function used to reduce the model complexity is expressed as:

$$r_{ij} = \begin{cases} 0, & (C_i \leq S_{ij-1} \text{ or } C_i \geq S_{ij-1}) \\ \frac{C_i - S_{ij-1}}{S_{ij} - S_{ij-1}}, & (S_{ij-1} < C_i < S_{ij}) \\ \frac{S_{ij+1} - C_i}{S_{ij+1} - S_{ij}}, & (S_{ij} < C_i < S_{ij+1}) \\ 1, & (C_i = S_i) \end{cases}$$

where r_{ij} is fuzzy membership of indicator i to class j , C_i is concentration value, and S_{ij} represents standard value of each water quality indicator or parameter.

To calculate the water quality index, weight (w_i) of each parameter has to be assigned based on its relative significance in controlling the overall water quality for human use. Maximum weight 5 is assigned to NO_3 and F due to their health hazard like blue-baby syndrome, fluorosis, respectively. HCO_3 and PO_4 are assigned minimum 1, because of either generally present in less concentration or

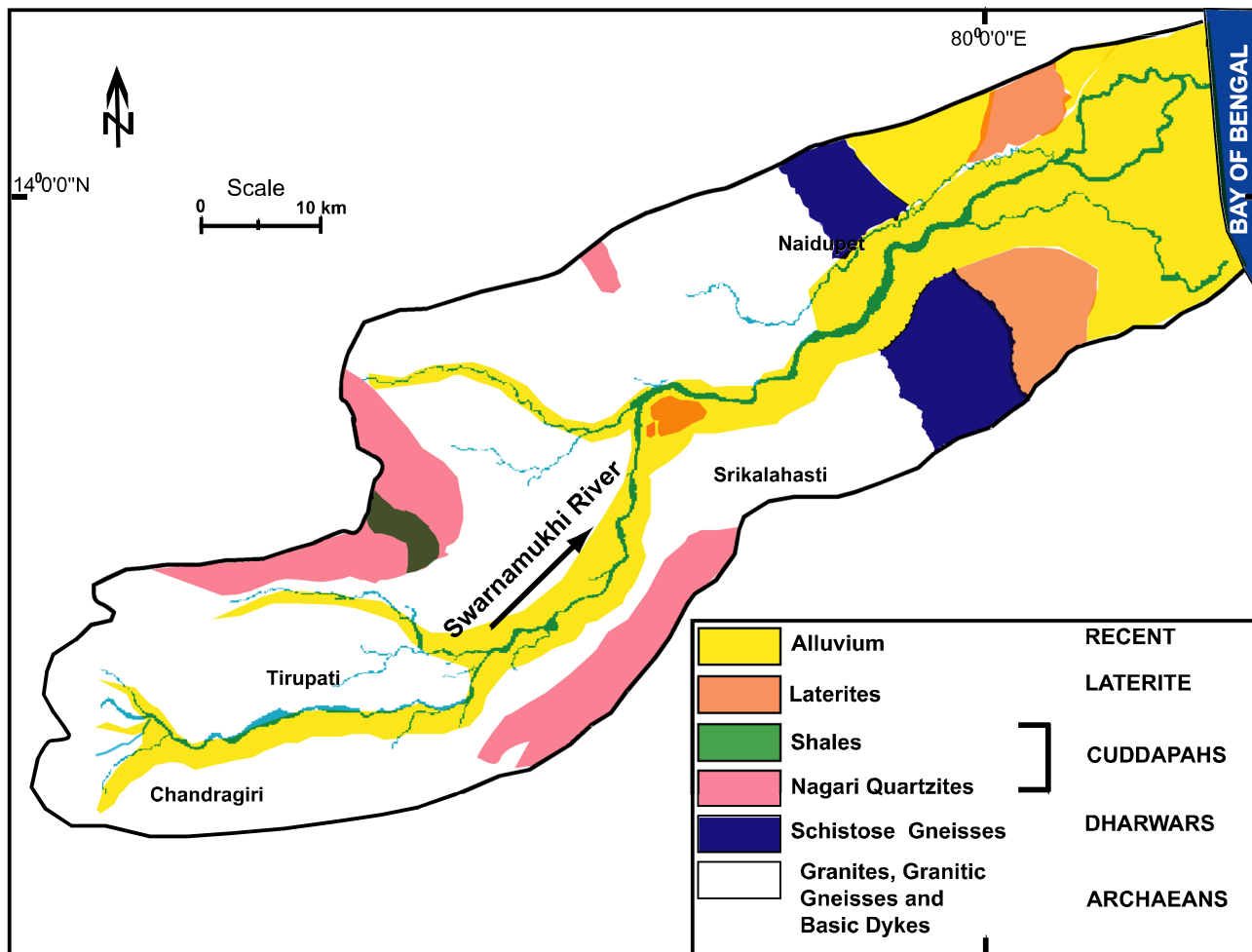


Fig. 2 Geology map of the study area

lesser impact on human health. The normalized weight of each parameter is expressed as:

$$W_i = \frac{w_i}{\sum_{i=1}^n w_i}$$

where w_i is weight, W_i represents normalized weight of parameter i , and $\sum_{i=1}^n w_i$ denote a sum of weight to all water quality parameter.

After getting normalized weight, quality rating is calculated by the following equation:

$$q_i = \left(\frac{C_i}{S_i} \right) \times 100$$

where q_i is quality rating, C_i is analytical value of water quality parameter i (mg/l), and S_i is permissible drinking water standard.

Water quality index (WQI) is the summation of obtained normalized weight of indicator (W_i) and quality rating (q_i) represented in equation:

$$WQI = \sum_{i=1}^n \left(\frac{w_i}{\sum_{i=1}^n w_i} \right) \times \left(\frac{C_i}{S_i} \right) \times 100$$

Mixing model is based on conservative mixing of sea/saline water with fresh groundwater. $\%f_{sea}$ is used to quantify similarity of seawater constituents with freshwater expressed as (meq/l):

$$\%f_{sea} = \frac{C_{cl,sample} - C_{cl,fresh}}{C_{cl,sea} - C_{cl,fresh}} \times 100$$

where f_{sea} is % of seawater fraction and $C_{cl,sample}$, $C_{cl,fresh}$ and $C_{cl,sea}$ are measured chloride in sample, freshwater and seawater. In the present study, mean of samples with high Ca, HCO_3 and correspondingly low Na, Cl and EC considered as freshwater, whereas seawater corresponds to analyzed Bay of Bengal water.

The quantification of ionic concentration change in freshwater on encounter with seawater can be evaluated by calculating theoretical composition ($C_{i,mix}$), based on

theoretical mixing of freshwater and seawater, followed by comparing the measured salinized groundwater sample with calculated theoretical composition expressed as (meq/l):

$$C_{i,mix} = f_{sea} \times C_{i,sea} + (1 - f_{sea}) \times C_{i,fresh}$$

or

$$C_{i,mix} = \left(\frac{C_{cl,sample} - C_{cl,fresh}}{C_{cl,sea} - C_{cl,fresh}} \times 100 \right) \times C_{i,sea} + \left\{ 1 - \left(\frac{C_{cl,sample} - C_{cl,fresh}}{C_{cl,sea} - C_{cl,fresh}} \times 100 \right) \right\} \times C_{i,fresh}$$

where $C_{i,mix}$ is theoretical concentration of ions for the theoretical mixing of freshwater–seawater and $C_{i,sea}$ and $C_{i,fresh}$ are seawater and freshwater concentration of each ion.

Change in concentration (ionic deviation) is related to comparison of a measured concentration of each ion to its theoretical calculated concentration in the mixture of freshwater and seawater which can be evaluated by the following equation (Fidelibus 2003):

$$\Delta C_i = C_{i,sample} - C_{i,mix}$$

where ΔC_i is ionic deviation of each ion and $C_{i,sample}$ is measured concentration of each ion in groundwater samples.

Saline water mixing index (SWMI) is applied for the delineation of saline water invasion regions of an area, formulated by Park et al. (2005). To calculate the index, four major chemical parameters of saline water are used as follows (mg/l):

$$SWMI = a \times \frac{C_{Na}}{T_{Na}} + b \times \frac{C_{Mg}}{T_{Mg}} + c \times \frac{C_{Cl}}{T_{Cl}} + d \times \frac{C_{SO_4}}{T_{SO_4}}$$

where SWMI is saline/seawater mixing index and C and T are measured and threshold concentration of ions in the groundwater samples, respectively. Constants a , b , c and d are relative concentration proportion of Na, Mg, Cl and SO_4 in seawater, respectively. Mondal et al. (2011) have calculated constant values ($a = 0.31$, $b = 0.04$, $c = 0.57$, $d = 0.08$) for saline water of the Bay of Bengal which is applied in this study. Threshold values of major ionic constituents are derived from cumulative probability curves which are site specific. Cumulative probability distribution is an important statistical tool to segregate the anomalous group from the entire groundwater samples whose chemistry is severely influenced by local activities leading to salinization and anthropogenic pollution with respect to natural background data. Intersection or inflection points of two neighboring linear population provide the threshold values in a log-probability plots (Lepeltier 1969; Sinclair 1974). Thus, cumulative probability

distribution is constructed against the abovementioned ions in a log concentration (mg/l) to reveal the threshold values of selected ions. In cumulative distribution plots, inflection point with lower concentration and below potable water drinking standards (WHO 1997) is used as natural background threshold value for corresponding ions.

Results and discussion

Hydrogeochemical data

Analytical results of the measured physico-chemical parameters and heavy metals for groundwater samples are presented in Table 1. The variation in parameters over time was analyzed using the box and whisker plots as shown in Fig. 3. Ca, Na, HCO_3 and Cl showed the high variance in the concentration distribution in both years. In pre- and post-monsoon 2014, Na predominates over Ca with high data variations but slight variation in Mg and K; however, in 2015, there is almost reverse occurred and Ca predominates over Na might be due to cation exchange process. SO_4 , NO_3 and F in both years showed similar trend with no temporal variation. Temporal variation could be observed in HCO_3 and Cl (2014–2015); Cl concentration (or median value) has increased with declining trend of HCO_3 . Thus, Ca, Na, HCO_3 and Cl are the principal ions which control the hydrogeochemistry of the study area. In 2015, HCO_3 and Cl concentration showed the difference between median and maximum values, suggesting natural and anthropogenic contamination inputs to the groundwater (Jiang et al. 2009; Devic et al. 2014). Groundwater quality classification based on hardness (Fig. 4) shows that majority of the samples are hard fresh type followed by hard brackish type; however, few samples also fall in soft freshwater category (Sawyer et al. 1994).

In heavy metals, Fe shows high variance and most of the samples are having concentration higher than median values. Around 52, 48, 50 and 47 % samples are exceeding the prescribed limit of WHO (2006) in pre- and post-monsoon seasons of 2014 and 2015, respectively. Heavy contamination of Fe may be due to dissolution of ferruginous minerals and domestic sewage seepage in the groundwater (Raju et al. 2011). Chromium is exceeding in few samples (20, 19, 22 and 23 % in pre- and post-monsoon of 2014 and 2015, respectively) due to widespread brick kilns, paints and wood preservatives. It causes damage to nervous system, fatigue and irritability in humans. Only few samples are exceeding the Mn prescribed limit due to Mn bearing minerals dissolution or sewage discharge. Study area is characterized by the absence of major industrial activities except ceramic and brick industries and, thus, can be interpreted that heavy metal could be from natural or other

Table 1 Statistical summary of chemical constituents and ionic ratios in the Swamamukhi river basin

Year Parameters	Pre-monsoon (2014)		Post-monsoon (2014)		Pre-monsoon (2015)		Post-monsoon (2015)	
	Range	Mean ± SD	Range	Mean ± SD	Range	Mean ± SD	Range	Mean ± SD
Ca ²⁺	38–306	115.8 ± 45.8	18–234	93.7 ± 50.8	40–320	139.1 ± 59.9	40–420	148 ± 85.2
Mg ²⁺	12–172.7	54.4 ± 32.2	13.4–226.7	75.0 ± 35.5	5–180	50.0 ± 34.2	3.4–200.7	54.7 ± 36.2
Na ⁺	43.1–459.7	204 ± 106.5	7.7–456.6	180.1 ± 96.3	21–442	171.1 ± 112.6	17–341	160.8 ± 79.5
K ⁺	0.8–277	15.0 ± 37.1	0.3–200.7	10.1 ± 26.1	0.4–156.6	11.4 ± 24.0	0.4–181.3	10.6 ± 24.7
CO ₃ ²⁻	0–39.3	2.9 ± 9.3	0–31.7	0.7 ± 4.3	0–118	14.9 ± 21.0	0–19	0.7 ± 3.0
HCO ₃ ⁻	120–1104	593.8 ± 245.6	72–960	471.2 ± 206.0	80–1100	469.1 ± 268.0	60–860	447.4 ± 207.8
SO ₄ ²⁻	4.5–63.1	26.9 ± 14.1	1.6–106.2	27.4 ± 17.7	1.7–60	26.8 ± 15.0	5.8–61.7	41.5 ± 14.4
Cl ⁻	140–1200	338.7 ± 182.3	96–1140	344.6 ± 171.5	100–940	345.4 ± 193.8	100–840	378.9 ± 169.2
PO ₄ ³⁻	0–1.9	0.1 ± 0.3	0–1.3	0.1 ± 0.2	0–1.9	0.1 ± 0.3	0.1–3.5	0.4 ± 0.6
F ⁻	0–1.9	0.4 ± 0.3	0.02–2.2	0.5 ± 0.4	0–1.7	0.3 ± 0.3	0–2.9	0.6 ± 0.5
NO ₃ ⁻	0–142.7	41.9 ± 27.4	0–150	47.4 ± 25.7	0–152.7	37.6 ± 31.8	0.9–472	41.7 ± 72.6
SiO ₂	0–25.8	10.8 ± 6.2	12.6–58.6	42.3 ± 9.2	0.1–43.5	14.4 ± 10.0	9.7–47.8	25.7 ± 8.3
Hardness	190.8–1146.1	512.5 ± 208.3	100–1176	542.7 ± 222.7	150.2–1138	552.6 ± 224.9	138.8–1403.3	626.4 ± 278.0
pH	6.4–8.6	7.2 ± 0.6	6.44–8.8	7.3 ± 0.4	6.6–8.8	8.0 ± 0.5	6.3–8.6	7.5 ± 0.5
EC	216–5080	172 ± 986.7	293–4140	1525.8 ± 840.3	299–3660	1464.1 ± 836.2	221–3120	1373.7 ± 698
TDS	120–2822.2	956.7 ± 548	163–2300	847.7 ± 466.8	175.9–2152.9	861.2 ± 491.9	130–1835.3	808.0 ± 410.6
Mn*	0–1599.2	61.9 ± 229.8	0–1065.8	58.6 ± 145.6	0–1674	63.9 ± 240.9	0–1987.7	102.9 ± 283.8
Cu*	0–539.3	75.6 ± 63.8	0–186	26.7 ± 37	0–453	68.7 ± 59	0–175	22.9 ± 36
Zn*	0–3996.4	337.4 ± 686.6	0–10,000	477 ± 1371.2	0–4021	361.4 ± 753.7	0–7000	559.7 ± 1312
Fe*	52.8–42,000	2166.5 ± 5574	0–18,046.2	1946.8 ± 3890	0–34,000	1975.7 ± 4632	0–21,978	2181 ± 44,450
Cr*	0–241.6	45.8 ± 64	0–250	41.3 ± 62.1	0–275	43.2 ± 64.3	0–231	45.7 ± 62
Ca/Na	0.1–1.3	0.4	0.04–4.6	0.4	0.1–2.7	0.7	0.1–3.0	0.8
Cl/NO ₃	2.6–120.2	12	3.2–59.1	9.2	1.9–99.6	19.4	0.7–240	45.2
Na/Cl	0.3–2.5	0.1	0.1–1.7	0.8	0.2–2	0.8	0.2–2.3	0.6
Mg/Ca	0.2–4.3	0.8	0.4–6.2	1.7	0.1–2.3	0.7	0.1–2.7	0.7
SO ₄ /Cl	0.02–0.2	0.12	0.01–0.6	0.10	0.01–0.4	0.10	0.03–0.3	0.13
f _{sea}	(–0.5) to 7.9	1.1	(–1.2) to 7.1	0.8	(–1.3) to 7.9	1.4	(–1.9) to 6.4	1.2
ΔCa	(–92.3) to 5.5	–14.5	(–138) to 18.3	–16.8	(–141.0) to 18.9	–25.73	(–96.4) to 26.5	–22.2
ΔMg	(–217.5) to 12.7	–30.4	(–212) to 33.8	–24.2	(–267.4) to 44.5	–46.43	(–209.2) to 57.3	–41.5
ΔNa	(–4705) to 286.5	–652	(–4195.9) to 719.2	–449.4	(–4713.4) to 797.2	–812.25	(–3786.5) to 1103.5	–740.2
ΔHCO ₃	(–8.9) to 52.1	8	(–33.1) to 15.4	3.9	(–15.3) to 50.6	7.71	(–24.2) to 46.1	6.9
ΔSO ₄	(–8.3) to 0.6	–1.1	(–6.8) to 2.1	–0.8	(–8.6) to 1.9	–1.45	(–3.0) to 0.5	–0.8
SWMI	0.61–4.66	1.76	0.69–6.04	2.08	0.35–3.39	1.38	0.50–3.89	2.19

All ions, TDS, SO₄/Cl, Cl/NO₃ in mg/l, EC in μS/cm, Ca/Na, Na/Cl, Ca/Na, Mg/Ca in mmol/l

* Heavy metals in μg/l

Fig. 3 Box-whisker plot for identification of physiochemical parameters

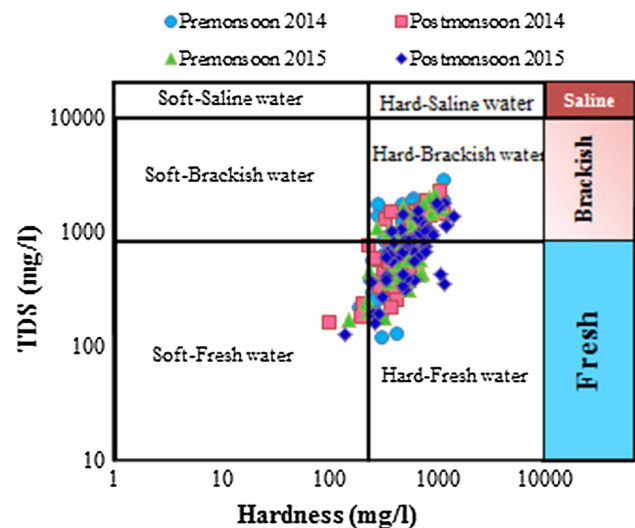
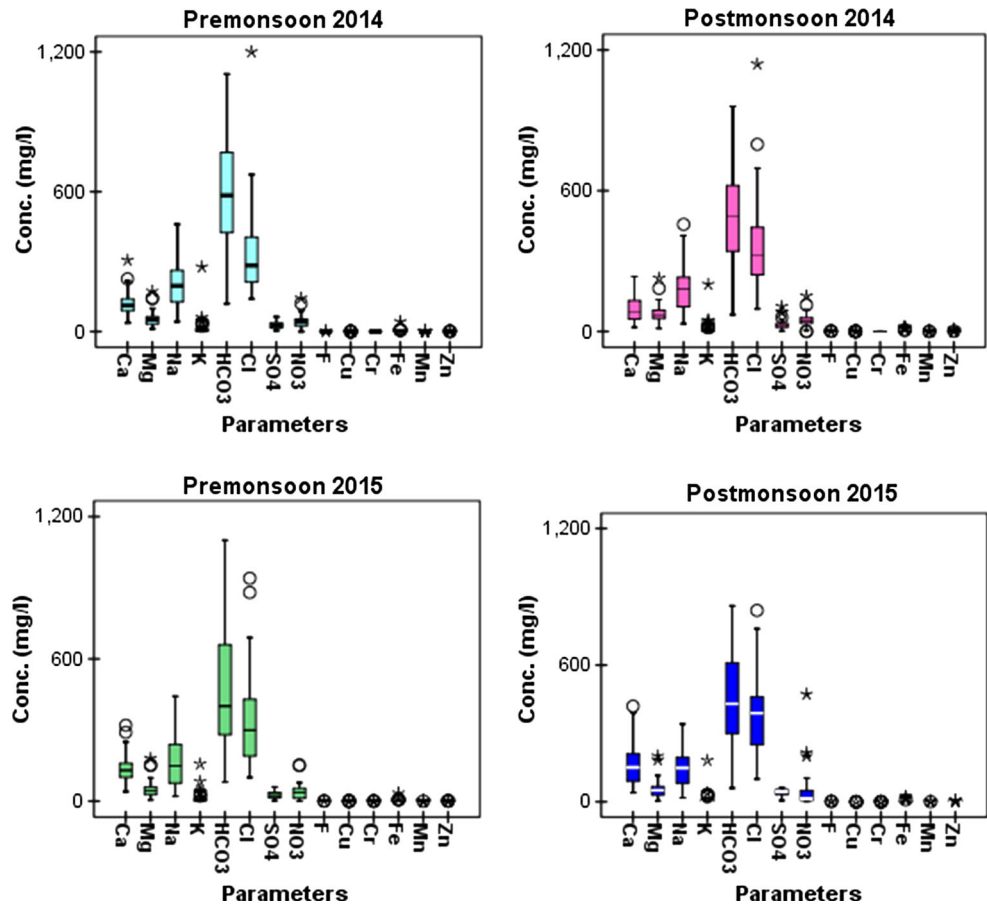


Fig. 4 Classification of groundwater quality based on TDS and hardness

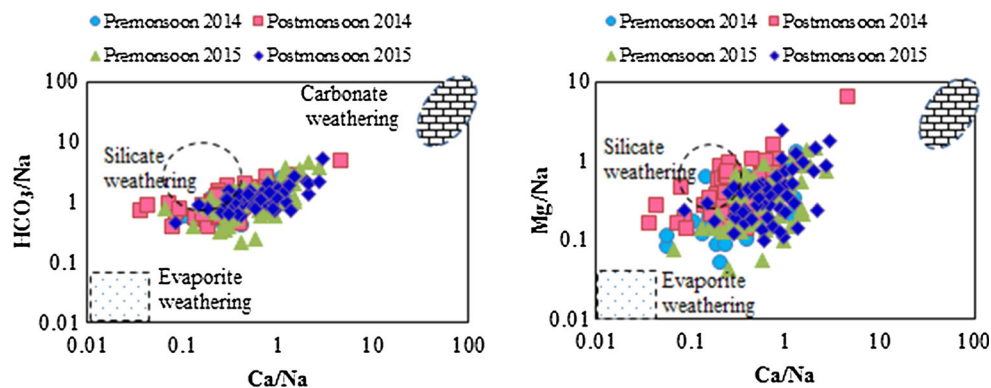
anthropogenic path. The order of cation abundance (mg/l) is: Na > Ca > Mg > K in both seasons of 2014 and Ca > Na > Mg > K in both seasons of 2015 and anion abundance: HCO₃ > Cl > NO₃ > SO₄ > CO₃ > F > PO₄ in both seasons of 2014 and 2015. The order of heavy metal

dominance (µg/l) is: Fe > Zn > Cu > Mn > Cr in pre-2014, Fe > Zn > Mn > Cr > Cu in post-2014, Fe > Zn > Cu > Mn > Cr in pre-2015 and Fe > Zn > Mn > Cr > Cu in post-monsoon 2015.

Source and processes identification

Various ionic ratios to reveal the specified source of ionic constituents of the groundwater are summarized in Table 1. Water-rock interaction comprises of three major lithological processes, i.e., evaporite, silicate and carbonate weathering. The logarithmic bivariate plots between molar ratios Ca/Na versus HCO₃/Na and Ca/Na versus Mg/Na are used to estimate the type of weathering (Fig. 5). Average Ca/Na ratio of crustal continental rocks is around 0.6 (Taylor and McLennan 1985). Higher solubility of Na than Ca increases the Na concentration; thus, Ca/Na ratio is expected to lower, imparting the silicate weathering as dominant geochemical process in the system (Gaillardet et al. 1999; Raju 2012; Zhu et al. 2014). In the plot Ca/Na versus HCO₃/Na, silicate weathering has been identified as major process; however, few data sets are also pointing toward the carbonate weathering. Mean value of Ca/Na ratio suggests the silicate weathering predominance. Ca/Na

Fig. 5 Dissolved phase diagrams of groundwater using Na-normalized molar ratios

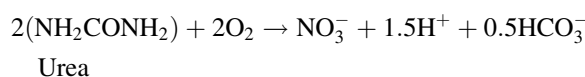


versus Mg/Na plot also denotes the predominance of silicate weathering followed by carbonate and evaporite dissolution. Few data points of pre-monsoon indicate evaporite dissolution due to semiarid climatic conditions. However, post-monsoon samples of both years shift toward carbonate dissolution due to heavy rainfall-driven calcite (lime kankar) and dolomite weathering process. The moderate to good positive regression between Ca/Na and HCO_3^-/Na ($R^2 = 0.45, 0.73, 0.59$ and 0.55 in pre- and post-monsoon of 2014 and 2015, respectively), Mg/Na and Ca/Na ($R^2 = 0.42, 0.85, 0.40$ and 0.30 in pre- and post-monsoon of 2014 and 2015, respectively) suggests the role of silicate weathering in influencing the hydrogeochemical constituent of the study area. Basin geological setup consists mainly of granites and granitic gneisses also confirming the silicate weathering source.

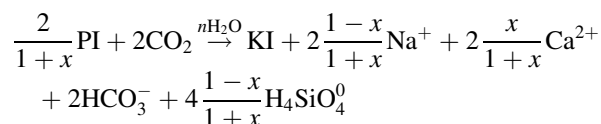
(Na + K) versus (Ca + Mg) plot clearly indicates that more points are below the equiline showing the abundance of alkaline earth element over alkali elements and could be due to ion exchange effect or dissolution of alkaline earth minerals (Fig. 6a). The temporal variation can be seen in this plot, as number of points has shifted below the equiline in post-monsoon 2015. Significant simultaneous increase of alkali elements (Na + K) with (Cl + SO_4) suggests a common source of these ions and presence of Na_2SO_4 , K_2SO_4 , NaCl and KCl in soil system (Fig. 6b) (Bhardwaj et al. 2010). Some of the sample points (mainly in pre- and post-monsoon 2015) deviate toward (Cl + SO_4) indicating other sources like silicate weathering, ion exchange or human activities for enrichment of alkalis in groundwater system. (Ca + Mg) versus Cl (Fig. 6c) and Na/Cl versus Cl (Fig. 6d) plot shows that increased salinity (Cl) is associated with increase in Ca + Mg and decrease in Na/Cl and could be due to ion exchange process in groundwater which adsorbs Na onto aquifer matrix in exchange for Ca + Mg.

Nitrate is an anthropogenic ion form by NH_4 bacterial conversion via nitrification under oxic conditions (Salman et al. 2014; Toumi et al. 2015). Of various ionic components of N, NO_3^- is the important water quality parameter which is also required by plants as growth

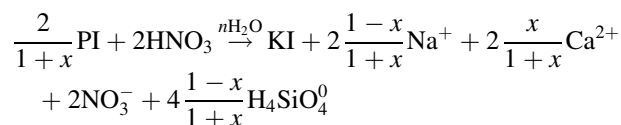
nutrient. N-fertilizer application enhances the mineral weathering because, in N-cycle, during nitrification process, proton (H^+) releases are represented as:



Proton (in form of HNO_3) resulting from nitrification would compete with proton generated from CO_2 (atm.) dissolution (in form of H_2CO_3) for the weathering of rock-forming minerals like plagioclase and granite (Semhi et al. 2000; Junior et al. 2014). With carbonic acid, the weathering of plagioclase producing kaolinite is represented as the following reaction:

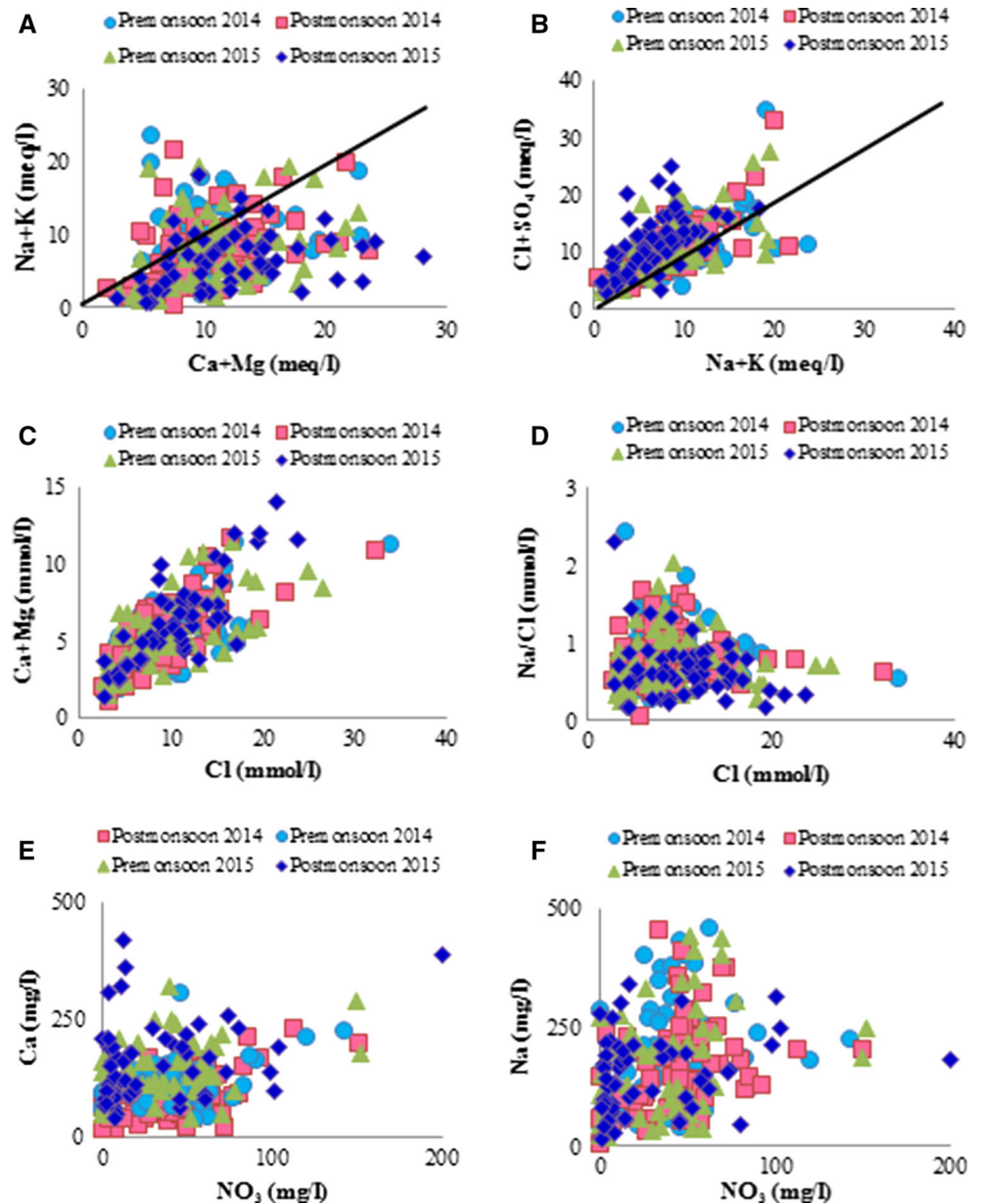


When weathering agent changes to nitric acid, the reaction becomes:



where PI = Plagioclase and KI = Kaolinite and x is the anorthite content of plagioclase. According to the above equations, if proton releases from nitrification process (Na and Ca would be balanced by NO_3^-), ionic constituents would increase and result in high TDS in nitrate-contaminated area apart from the contribution of carbonic acid-driven weathering. The plot of NO_3^- versus Ca and NO_3^- versus Na (Fig. 6e, f) shows Ca–Na increasing trend with NO_3^- in all studied seasons except post-monsoon 2015 indicating the significant effect of nitric acid-driven chemical weathering. One sample (48: Gandhinagar) has abruptly very high concentration of 472 mg/l NO_3^- which is discarded from the plots as it is not a representative sample. It is found that nitrate toward higher side in post- than in pre-monsoon of both years may be due to its high infiltrate

Fig. 6 Relationship between major ion concentrations
a Na + K versus Ca + Mg,
b Cl + SO₄ versus Na + K,
c Ca + Mg versus Cl, **d** Na/Cl versus Cl,
e Ca versus NO₃,
f Na versus NO₃



rate in soils. Some parts of Swarnamukhi river basin have lot of dumped municipal solid wastes which on degradation releases nitrate which seeps underground while recharging and, thus, can contaminate the groundwater of nearby wells. In addition to agricultural input and municipal solid waste, people offer lot of flowers, leaves and twigs while worshipping in the Hindu pilgrimage spots which were drained indiscriminately in open places or river where its degradation releases nitrate and contaminate groundwater. Coarse and alluvial soil allows rapid infiltration of nitrate due to high porosity, whereas clayey soils due to its high binding capacity restrict its movement and control the contamination (Raju et al. 2009). Clay particles have minute inter-pore spaces which leave less space for O₂;

thus, facultative bacteria utilize NO₃ as energy source instead of O₂, resulting in the denitrification process in a natural sustainable way to reduce the contamination. The study area is dominated by the alluvial soil system in which this type of self-purification system did not work and, thus, subsequently result in high NO₃ contamination. Nevertheless, Cl/NO₃ ratios are evaluated (mean values: 12, 9.2, 19.4 and 45.2 in pre- and post-monsoon seasons of 2014 and 2015, respectively) to quantify the nitrate degradation in groundwater system of both the years. Considering the ratio value of 4.9 as reference point of major river water (Majumder et al. 2008), it was found that majority of the wells have higher ratio values suggesting the proficient removal of nitrate by denitrification process.

The influence of cation exchange process is evaluated by $(Ca + Mg) - (HCO_3 + SO_4)$ versus $(Na + K - Cl)$ plot (Fig. 7). $Ca + Mg$ involvement in the process was corrected by subtracting $HCO_3 + SO_4$ that would be derived from carbonate and silicate weathering. $Na + K$ derived from aquifer matrix would be balanced by Cl salt dissolution. If these activities are prominent in the system, slope should be (-1) ($y = -x$) (Jankowski and Acworth 1997; Kumar et al. 2014). Slopes of the plot ($y = -0.98x, -1.02x, -0.99x$ and $-0.95x$ in pre- and post-monsoon of 2014 and 2015, respectively) suggest that cation exchange is playing a momentous part in controlling the hydrogeochemistry of the study area. It can also be observed that a good number of data points of pre- and post-monsoon 2015 fall in fourth quadrant which implies $Ca + Mg$ dominance over $Na + K$.

Geochemical modeling

CO_2 plays a critical role in controlling water quality because water saturated with CO_2 is aggressive weathering agent. Groundwater has additional supply of CO_2 from decaying organic matter in a soil zone apart from atmospheric contribution. It is interesting to note that pCO_2 in majority of the samples are higher than atmospheric value of $10^{-3.5}$ atm. This suggests the equilibrium state of water bodies with atmosphere and explains that aquifer system is open to soil CO_2 with capacity to dissolve silicates and carbonates. Thus, infiltration of fresh recharge water into the groundwater system dissolves carbonate minerals first followed by silicates due to its higher dissolution rate (Montcoudiol et al. 2014; Gueroui et al. 2014). Majority of the samples (83, 77, 98 and 84 % samples in pre- and post-monsoon of 2014 and

2015) (64, 77, 95 and 88 % samples in pre- and post-monsoon of 2014 and 2015, respectively) are saturated with respect to calcite and dolomite minerals, which indicates that the groundwater is saturated with carbonates resulting in a high Ca concentration, respectively (Fig. 8). Calcium increased in both the seasons of 2015 indicating toward the oversaturation of calcite and cation exchange process. Calcite precipitation is enhanced by common ion effect when Ca from gypsum or fluorite dissolution leads to increase Ca concentration, declining HCO_3 concentration and enrichment of Cl in groundwater (Molina-Navarro et al. 2014). Sulfate minerals (anhydrite and gypsum) undersaturated state shows the tendency of dissolution and further possibility of amplified SO_4 . This could be the reason for the lower concentration values of SO_4 in the groundwater system. Silica in the groundwater is found in lower concentration due to its less susceptibility toward weathering as indicated by saturation index values of silicate minerals present in the groundwater system. Chalcedony and quartz attain the dissolution state in pre- and near to equilibrium in post-monsoon of both the years.

Stability plot of silicate minerals is helpful in thermodynamic studies, defining various hydrogeochemical reactions (Stumm and Morgan 1996). Plotting of $Ca/H, Mg/H, Na/H$ and K/H on thermodynamic stability diagram as a function of H_4SiO_4 is shown in Fig. 9. Stability diagrams of Ca show kaolinite as a major weathered product from Ca -silicate minerals followed by Ca -montmorillonite and gibbsite clays.

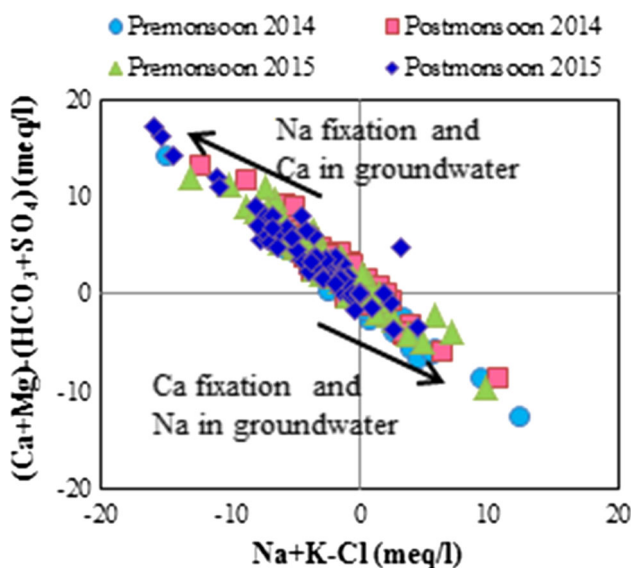
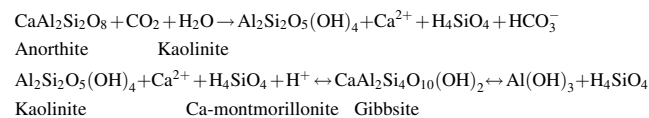


Fig. 7 Bivariate cation exchange plot of $Na + K - Cl$ and $(Ca + Mg) - (HCO_3 + SO_4)$

In Ca system plot, few samples of post-2014 and pre- and post-monsoon 2015 are shifting from kaolinite to Ca -montmorillonite field, explaining the dissolution of Ca -rich minerals in the groundwater (Raju et al. 2012). Restricted groundwater flow in semiarid conditions favors strong interaction of groundwater-silicate mineral (long residence time), resulting in montmorillonite formation. It is also observed that one sample of pre-monsoon 2014 and 2015 is in final stage of weathering and forms gibbsite with the further loss of silica. Majority of the samples on right side of line for quartz suggests its saturation or equilibrium state as shown in saturation indices; thus, excess Si in the groundwater could be from amorphous Si . In Mg system, formation of kaolinite, chlorite and gibbsite mineral occurs in both the years. Mg silicates in dissolution phase form these clay minerals and release Mg into groundwater. In stability plot of Mg system, shift has been observed from kaolinite to chlorite in pre- and post-monsoon 2014 and 2015, due to excess supply of cations and Si helps in forming new clay mineral.

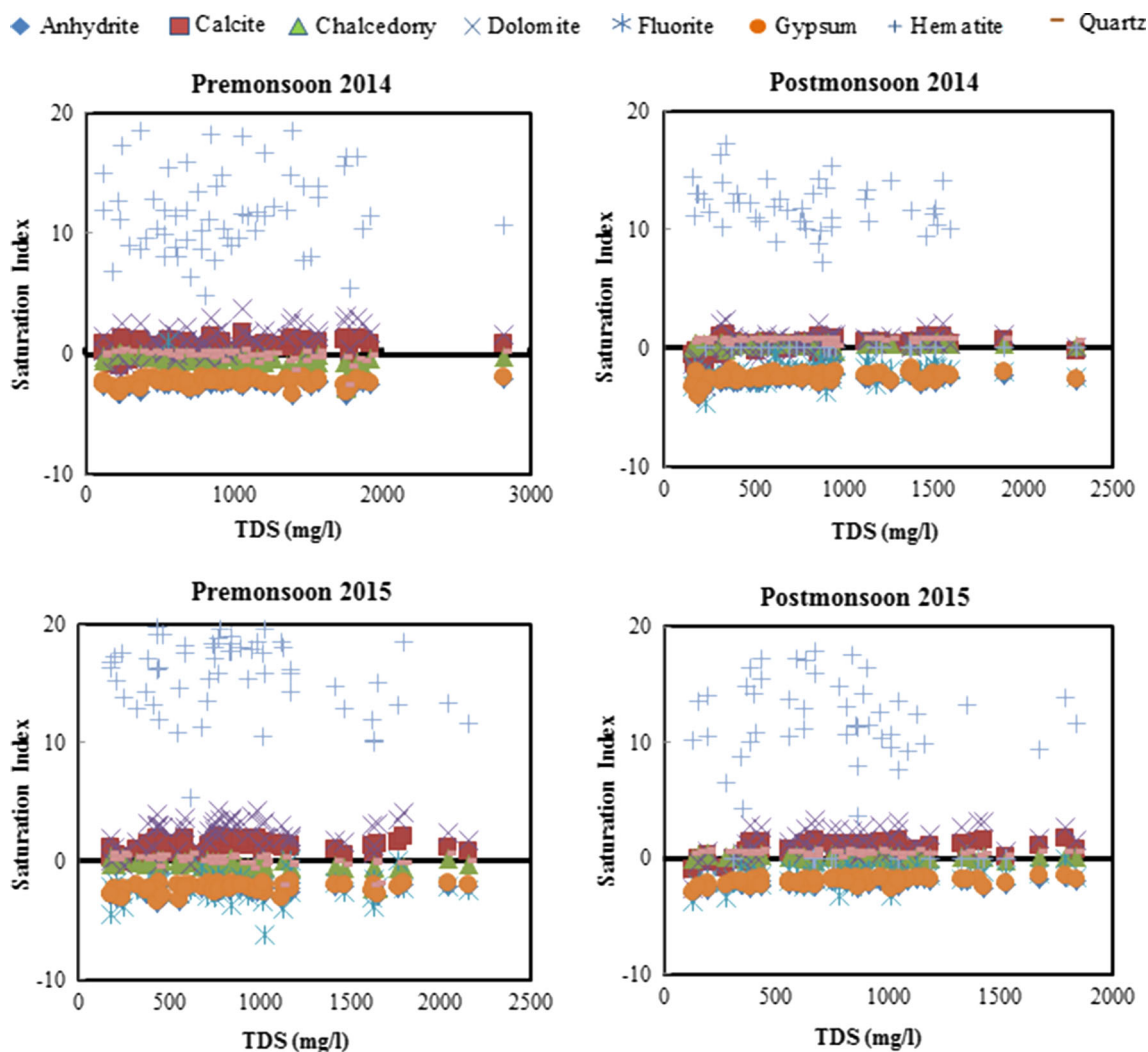
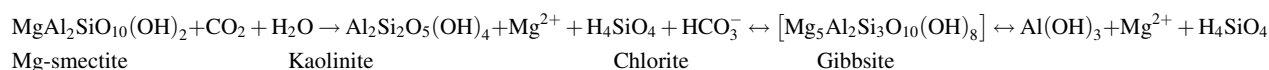
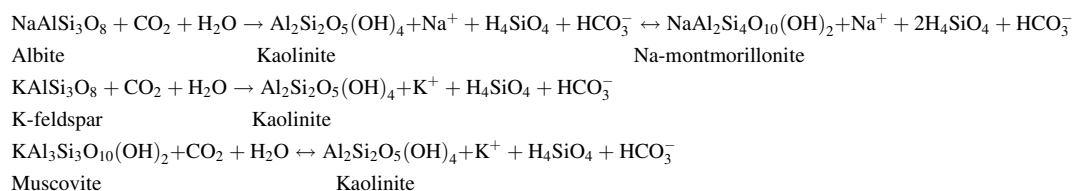


Fig. 8 Plot of saturation indices of different minerals with respect to TDS



Mineral stability diagram of Na imparts the dominance of kaolinite; however, one sample of pre-monsoon 2014 and 2015 forming the gibbsite might be due to high aridity conditions in the study area. It indicates the incongruent dissolution of albite

to form kaolinite and other secondary products (Rajmohan and Elango 2004). In pre-monsoon 2015, fewer sampling points are showing shift toward montmorillonite field due to progressive dissolution of albite which increases Na and Si values.



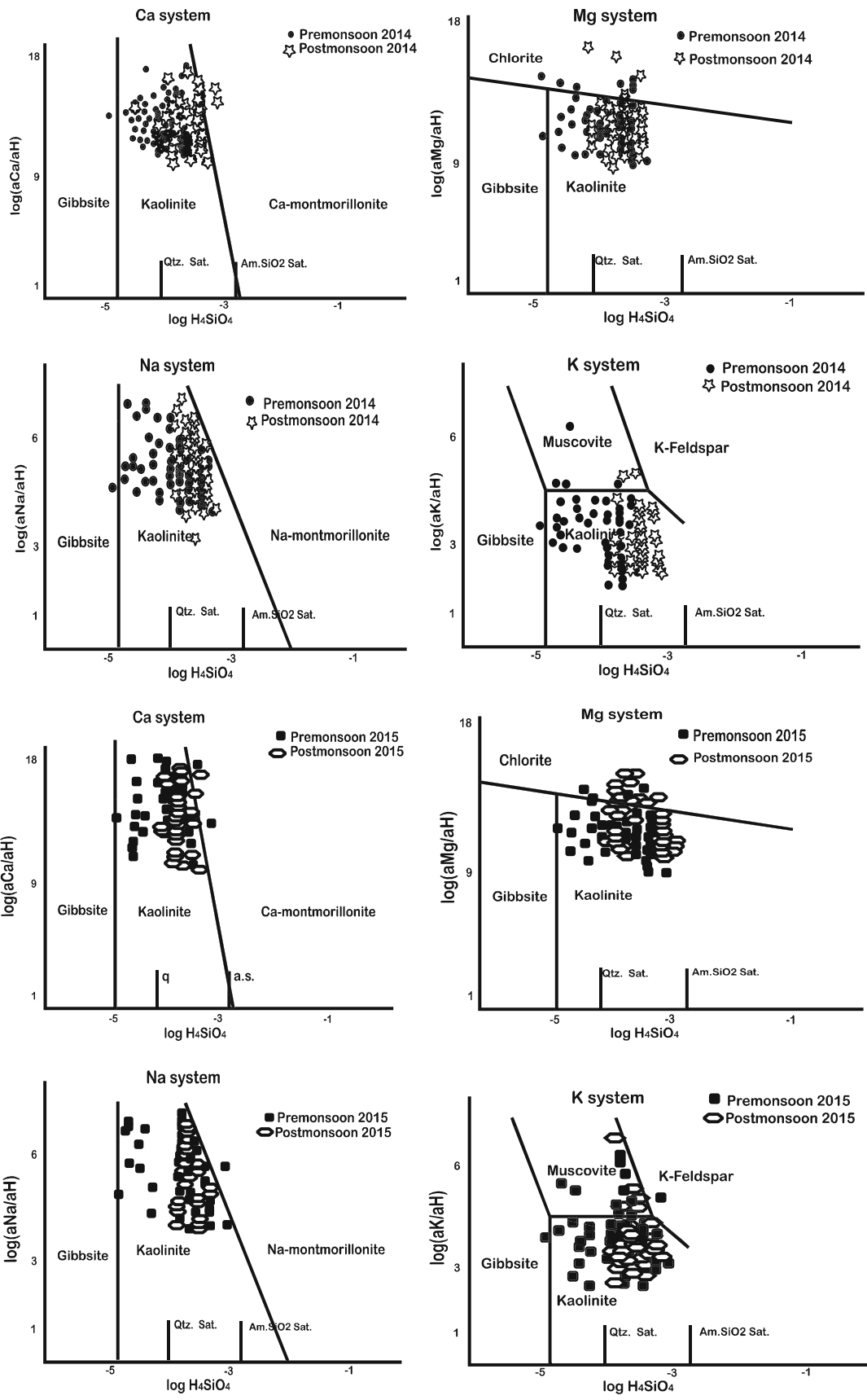


Fig. 9 Thermodynamic stability plots of different ionic ratios as a function of H_4SiO_4

In K system, majority of the sample points fall in kaolinite field, while few points cluster to the boundary of kaolinite and K-feldspar zone in both the years.

Factor analysis

Factors and their eigenvalue, % variance and % cumulative are presented in Table 2. For the better understanding of derived factors (1 and 2) a simplified bivariate plots of both the seasons of 2014 and 2015 are prepared to deduce the major prevailing sources in enrichment of ions in the groundwater (Fig. 10). Sources can be of three types: natural, anthropogenic or mixed (water–rock interaction, anthropogenic influences, atmospheric contribution, sea water intrusion and cation exchange process) which typically control the hydrogeochemistry of an area.

According to the plot, ions (Ca, Mg, Na, NO_3 and Cl) and general parameters (hardness and EC) are contributed by mixed sources in both the seasons of 2014. Dissolution of minerals releases Ca, Mg and Na and specifies water–rock interaction for enrichment of these ions in the groundwater. Significant influence of ill-human activities such as heavy usage of agricultural fertilizers, agricultural runoff water, wastewater reuse, unlined sewage waste and municipal waste contributes NO_3 , Na and Cl in appreciable amount. Nitrification process also leads to weathering and releases Ca, Mg or Na in groundwater. Small amounts of Ca are incorporated in the *N*-fertilizers as plant nutrients in form of $Ca(NO_3)_2$ (Zghibi et al. 2014). High loading of Mg directs toward the seawater intrusion in the coastal aquifers of basin present along the Bay of Bengal. In 2015, high loading of Ca, Na, Cl and SO_4 imparting the role played by mixed sources such as $CaCl_2$, NaCl, $CaSO_4$ and Na_2SO_4 mineral weathering, municipal wastewater along with cation exchange between Ca and Na in both the seasons. Post-monsoon seasons of both the years show higher loading of HCO_3 apart from other ions suggesting the active weathering process and recharge activities. Higher loading (>0.9) of K and PO_4 in second factor signifies their common anthropogenic source in all studied seasons. Fertilizers contain nitrogen, phosphorus and potassium in different ratios whose excess application leaves behind *N*, *P* and *K* in field and drain to runoff which further contaminate groundwater. These three ions acquire different chemistry; thus, they may not reach the groundwater at the same time and show anomalous presence. Domestic waste, sewage wastewater, animal excreta and pit latrines also contribute these ions in groundwater of the basin area. In pre-monsoon 2015, positive loading of CO_3 apart from K

and PO_4 suggests the high rate of decomposition of human-sourced waste matters.

In factor 3, positive loading of pH and CO_3 explains 9.22 and 11.34 % of total variance in pre- and post-monsoon 2014, respectively. pH indicates about the alkaline behavior which could arise by carbonate mineral weathering (lime kankar) or organic matter degradation by soil organisms releasing lot of carbonates and suggesting their natural source. In 2015, Mg, HCO_3 and NO_3 explain 8.84 % variance in pre- and Na and Si explain 9.81 % variance in post-monsoon. In pre-monsoon 2015, dolomite weathering is influenced by nitrification, and noticed positive Ca and negative Si loadings indicate low impact of silicate weathering for Ca enrichment. In post-monsoon 2015, significant relation between Na and Si is indicative of natural geogenic source, i.e., weathering of silicate minerals.

Factor 4 reflects positive loading of HCO_3 , F and Si and negative loading of SO_4 with 7.89 and 7.72 % of total variance in pre- and post-monsoon of 2014, respectively. Positive relations of these ions deduce the dominance of silicate weathering. Si presence is justified by the geological setup of the basin area and saturation index values. The weathering of aluminosilicate minerals releases HCO_3 , which further eases the fluorite dissolution especially in alkaline ambience.



Negative loading shows the insignificant contribution of SO_4 in controlling the hydrogeochemistry of the basin area. In 2015, positive loading of pH, F, Si and negative loading of Ca explain 7.84 % variance in pre-monsoon and positive loading of CO_3 , F and pH explains 7.89 % of variance in post-monsoon. Interactions between fluorite and groundwater for a long period of time indicate the enrichment of fluoride, and negative relation of Ca with F is due to the removal of Ca by calcite precipitation (Raju et al. 2012).

Hierarchical cluster analysis (HCA)

Hierarchical cluster analysis applied over the hydrogeochemical data, and obtained results are shown as dendrogram, from which different hydrogeochemical groups can be identified (Fig. 11). Representative stiff diagram of major ions is plotted for each cluster for easy identification of similarity or differences between them (Table 3).

Cluster 1 (C1) of pre-monsoon 2014 represents low mineralized water with low EC (mean: 1174 $\mu S/cm$) and $Na-HCO_3 > Na-Cl > Ca-Cl > Ca-HCO_3 > Mg-HCO_3$ hydrogeochemical facies. Predominance of $Na-HCO_3$ over other facies imparts the dominance of silicate mineral weathering process which provide both ions in proportionate amount along with ion exchange and freshwater recharge. Cationic and anionic facies as per the Stiff

Table 2 Rotated component matrix of 16 chemical variables

Variables	1				2				3				4			
	2014		2015		2014		2015		2014		2015		2014		2015	
	Pre	Post	Pre	Post	Pre	Post	Pre	Post	Pre	Post	Pre	Post	Pre	Post	Pre	Post
Ca ²⁺	0.75	0.64	0.57	0.83	-0.30	-0.10	-0.02	0.03	-0.29	-0.34	0.11	-0.34	-0.10	0.45	-0.56	0.08
Mg ²⁺	0.72	0.80	0.31	0.58	-0.08	-0.18	-0.09	0.15	-0.17	0.08	0.76	0.20	0.41	0.08	-0.15	-0.03
Na ⁺	0.58	0.73	0.73	0.53	0.30	0.34	0.18	0.39	0.36	0.02	0.37	0.65	0.29	-0.44	0.36	-0.04
K ⁺	0.04	0.10	0.04	0.03	0.92	0.92	0.85	0.82	0.12	-0.01	0.27	0.09	0.15	0.06	-0.08	0.28
CO ₃ ²⁻	-0.07	-0.07	0.16	-0.01	0.22	-0.03	0.72	0.37	0.81	0.84	-0.08	0.25	0.05	0.26	0.46	0.68
HCO ₃ ⁻	0.48	0.71	0.13	0.75	0.26	0.31	0.12	0.22	-0.01	-0.03	0.82	0.39	0.75	0.08	0.07	-0.18
Cl ⁻	0.87	0.90	0.92	0.81	0.07	0.02	0.06	0.10	0.13	-0.08	0.12	0.04	-0.11	-0.18	-0.16	0.30
F ⁻	-0.21	0.07	0.10	0.26	-0.27	-0.12	-0.03	0.03	0.27	0.06	-0.21	-0.05	0.61	0.84	0.77	0.62
PO ₄ ³⁻	-0.06	0.03	0.03	-0.12	0.91	0.90	0.90	0.78	0.12	-0.03	-0.03	-0.03	0.01	0.00	0.05	0.29
SO ₄ ²⁻	0.17	0.12	0.61	0.79	-0.14	-0.03	-0.28	0.16	-0.26	-0.05	0.00	0.12	-0.52	-0.72	0.13	-0.09
NO ₃ ⁻	0.51	0.50	0.28	0.35	0.10	0.20	0.06	0.62	-0.20	-0.21	0.52	-0.06	0.31	0.44	0.08	-0.40
Si	-0.37	0.15	-0.16	-0.04	-0.28	0.09	-0.12	0.09	-0.04	-0.33	-0.07	0.88	0.72	0.57	0.60	-0.09
pH	0.01	-0.12	-0.06	-0.07	0.03	-0.01	0.11	0.14	0.88	0.85	0.09	-0.02	0.07	-0.29	0.82	0.71
EC	0.90	0.95	0.82	0.80	0.17	0.20	0.19	0.35	0.14	-0.12	0.46	0.35	0.20	-0.10	-0.14	0.06
TDS	0.90	0.95	0.82	0.80	0.17	0.20	0.19	0.35	0.14	-0.12	0.46	0.35	0.20	-0.10	-0.14	0.06
Hardness	0.87	0.89	0.57	0.94	-0.22	-0.18	-0.07	0.06	-0.27	-0.14	0.56	-0.16	0.21	0.31	-0.46	0.04
Eigenvalue	6.03	6.22	5.90	6.07	2.98	2.01	2.60	2.57	1.48	1.82	1.41	1.57	1.26	1.23	1.30	1.26
% Variance	37.71	38.88	36.91	37.93	18.63	12.58	16.25	16.05	9.22	11.34	8.84	9.81	7.89	7.72	7.84	7.89
% Cumulative	37.71	38.88	36.91	37.93	56.34	51.46	53.32	53.98	65.56	62.80	62.00	63.79	73.45	70.52	70.20	71.6

Bold values are with Significance level alpha = 0.05

Fig. 10 Source identification plots of factor 1 versus factor 2

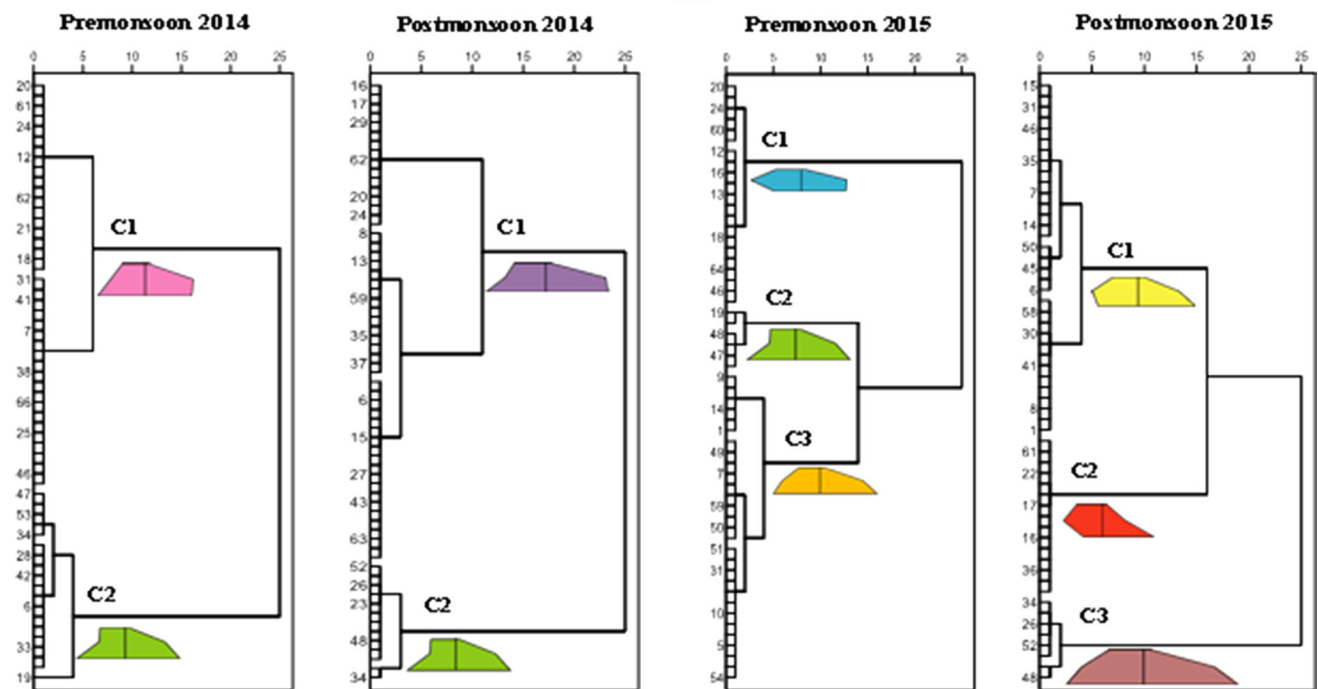
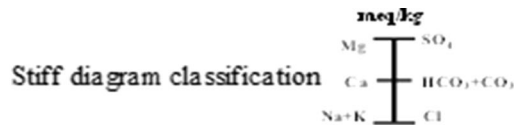
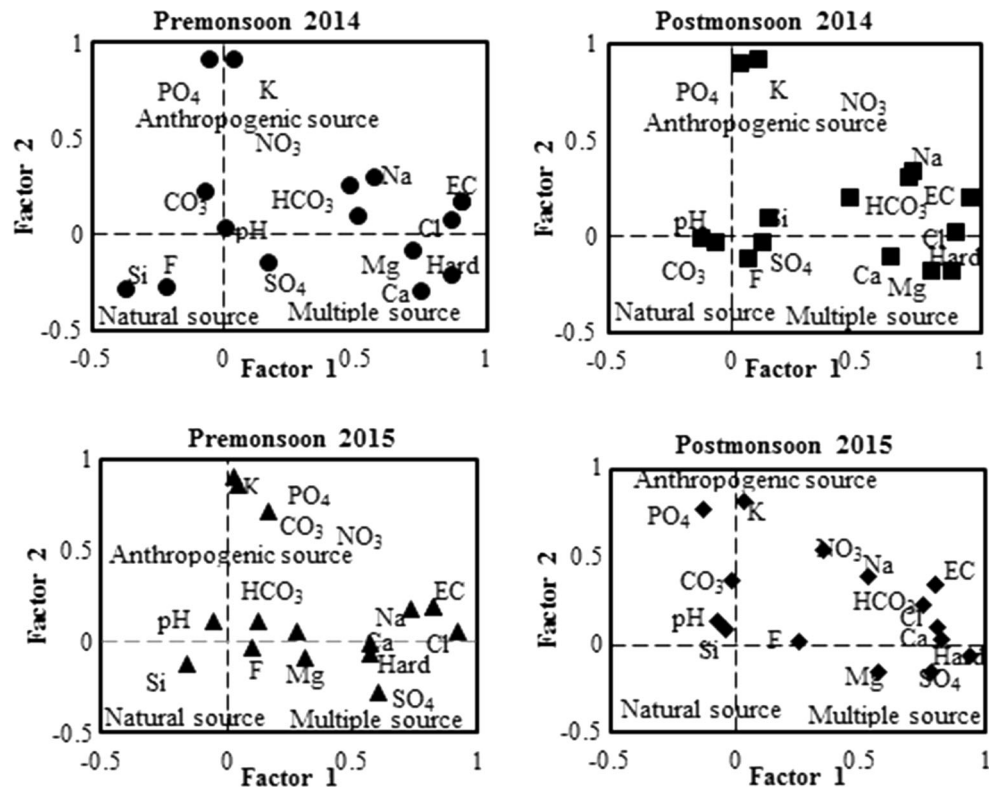


Fig. 11 Hierarchical cluster map showing dendrogram, clusters and stiff diagrams

Table 3 Characteristics of different classified clusters obtained by HCA

Cluster	2014						2015					
	Pre (N = 59)		Post (N = 66)		Pre (N = 57)		Post (N = 57)		Pre (N = 57)		Post (N = 57)	
	C1 (N = 40)	C2 (N = 19)	C1 (N = 53)	C2 (N = 13)	C1 (N = 21)	C2 (N = 6)	C3 (N = 30)	C1 (N = 34)	C2 (N = 15)	C3 (N = 8)		
Water facies (%)	NaHCO ₃ (30), NaCl (24), CaCl = CaHCO ₃ (20), MgHCO ₃ (3)	NaCl (47), NaHCO ₃ (32), MgCl (16), CaCl (5)	NaCl (28), NaHCO ₃ (24), MgCl (26), CaCl (11), MgHCO ₃ (9), CaHCO ₃ (2)	NaCl (55), MgCl = CaCl = NaHCO ₃ (15)	CaHCO ₃ (52), CaCl (43), NaHCO ₃ (5)	NaCl (59), NaHCO ₃ (41)	NaCl (35), NaHCO ₃ (25), CaCl (20), CaHCO ₃ (17), MgCl (3)	CaCl (41), NaCl (24), NaHCO ₃ (21), CaHCO ₃ (14)	CaCl (81), NaHCO ₃ (13), MgCl (6)	NaHCO ₃ (25), CaHCO ₃ (12)		
Mean values of ions obtained from different clusters												
EC	1174	2876	1206	2829	669	3127	1688	1446	545	2621		
Ca	106.43	135.5	82.2	140.5	113.8	176.7	149	169.2	111	218.8		
Na	156.8	303.4	153	290.8	66	350.5	207	161.8	60.2	253.7		
HCO ₃	518.9	751.5	420.2	679.1	319	815	503.1	496.5	220.7	663.8		
Cl	250	526	285.4	586	180	636.7	403.5	383.2	262.5	578.8		
NO ₃	34.1	58.26	43.2	64.2	25.4	74	34	39.2	16	100.3		

diagram follow the order of $Na > Ca \gg Mg$ and $HCO_3 > Cl \gg SO_4$, and groundwater of this group is safe for domestic and irrigation purposes. C2 of pre-monsoon 2014 identified as mineralized water with high EC (mean: 2876 $\mu S/cm$) and prevalence of $Na-Cl > Na-HCO_3 > Mg-Cl > Ca-Cl$ water facies. C1 and C2 of post-monsoon 2014 have $Na-Cl > Na-HCO_3 > Mg-Cl > Ca-Cl > Mg-HCO_3 > Ca-HCO_3$ with low EC and $Na-Cl > Mg-Cl = Ca-Cl = Na-HCO_3$ water facies with high EC, respectively. Decrease in $Na-HCO_3$ and increase in $Na-Cl$ water facies have been observed in post-monsoon 2014 which can be explained by inefficient freshwater recharge because of low rainfall and prevalent drought conditions resulting in high rate of evaporation. Thus, C2 of both the seasons of 2014 constitutes highly mineralized water which is unfit and needs treatment before domestic use.

In C1, pre-monsoon 2015, the groundwater has lower concentration of ions and represents $Ca-HCO_3 > Ca-Cl > Na-HCO_3$ water facies. $Ca-HCO_3$ water type may be due to carbonate, silicate weathering or recharge by freshwater. High Ca concentration also represents the efficient cation exchange process (Fig. 4). Stiff diagram of C1 pre-monsoon 2015 has similar shape with that of pre-monsoon 2014, but shift has been observed on the cation side between Na and Ca, indicating cation exchange prevalence. Thus, majority of the samples in 2014 are $Na-HCO_3$ which is replaced by $Ca-HCO_3$ -type water facies in 2015. C2 of pre-monsoon 2015 constitutes only 6 groundwater samples with highest EC (mean: 3127 $\mu S/cm$) of all the identified clusters indicating the long residence time of groundwater with aquifer material which result in high dissolution and higher ionic constituent. High EC could also be attained by various anthropogenic inputs like domestic sewage or agricultural ill practices. C3 of pre-monsoon 2015 constitutes $Na-Cl > Na-HCO_3 > Ca-Cl > Ca-HCO_3 > Mg-Cl$ water facies, and corresponding stiff diagram has different shapes compared to other C1 and C2 clusters. In the cation side, Ca and Na have fewer differences in their concentration which indicates mixed type of water facies. In C1 of post-monsoon 2015, the order of facies is $Ca-Cl > Na-Cl > Na-HCO_3 > Ca-HCO_3$ which implies the mixing of freshwater with saline water (Adams et al. 2001). In corresponding stiff diagram, anion side is almost similar to C3 of pre-monsoon 2015, but cation side takes a noticeable shift from Na to Ca. In C2 of post-monsoon 2015, the order of hydrogeochemical facies is $Ca-Cl > Na-HCO_3 > Mg-Cl$. Least sampling location is grouped in C3 of post-monsoon 2015 with high EC (mean: 2621 $\mu S/cm$), and the order of facies is $Na-HCO_3 > Ca-Cl > Na-Cl > Ca-HCO_3$. This cluster constitutes the maximum nitrate concentration (mean: 100.3 mg/l) suggesting severe NO_3 contamination making water not suitable for drinking or domestic usage.

Table 4 Water quality parameters and their assigned weights

Parameter	WHO permissible limit (1997)	w_i	W
TDS	1500	5	0.12
HCO_3^-	600	1	0.02
Cl^-	600	5	0.12
SO_4^{2-}	600	5	0.12
PO_4^{3-}	0.1	1	0.02
NO_3^-	50	5	0.12
F^-	1.5	5	0.12
Ca^{2+}	200	3	0.07
Mg^{2+}	150	3	0.07
Na^+	200	4	0.09
K^+	12	2	0.05
Σ		39	0.92

Fuzzy membership calculations

Groundwater samples have assigned the different classes according to obtained WQI (Tables 4, 5). It is found that majority of the samples (58, 36, 60 and 42 % samples in pre- and post-monsoon of 2014 and 2015, respectively) are clustered in Class I which is excellent for drinking purpose. Class I water indicates low mineralized water and no risk of groundwater contamination by NO_3 , F or Cl ions. Class II water represents good groundwater for drinking and agriculture usage and is found in 40, 62, 38 and 49 % samples in pre- and post-monsoon of 2014 and 2015, respectively. Class IV represents very poor water is a result of high residence time of groundwater which enrich the water with excess ions or strong influence of various anthropogenic activities. It is not recommended for human consumption or irrigation purpose. After classification, it is observed that the water quality is further deteriorated in post-monsoon in both the years which might be due to mixing of various surface anthropogenic wastes or evaporates with rainwater and infiltration while recharging the groundwater. Spatial distribution of water quality index shows the dominance of Class I water in the study area (Fig. 12). Major pocket of Classes III and IV is confined to extreme southwest region due to high rate of anthropogenic activities.

Salinization of the fresh groundwater: contaminants and processes

Salinization source identification

The Swarnamukhi river basin is vulnerable to salinity due to its urban flow and reaching up to Bay of Bengal. Chlorine ion helps to identify the origin and evolution of dissolved salts due to its stable character in water which is

Table 5 Classification of groundwater based on water quality index (% samples exceeding WQI classes)

Class	Range	Pre-monsoon 2014	Post-monsoon 2014	Pre-monsoon 2015	Post-monsoon 2015
Class I (excellent water)	<50	58	36	60	42
Class II (good water)	50–100	40	62	38	49
Class III (poor water)	100–200	–	2	2	7
Class IV (very poor water)	200–300	2	–	–	2
Class V (unsuitable for drinking)	>300	–	–	–	–

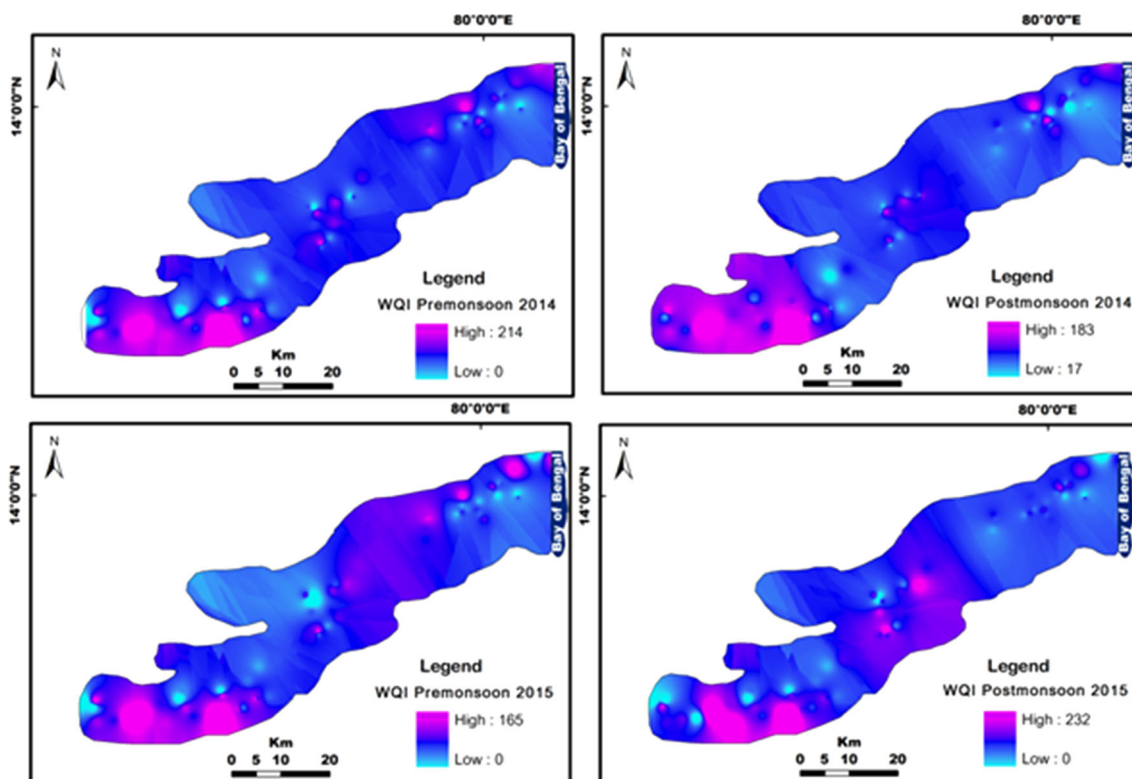


Fig. 12 Seasonal wise spatial distribution of water quality index (2014 and 2015)

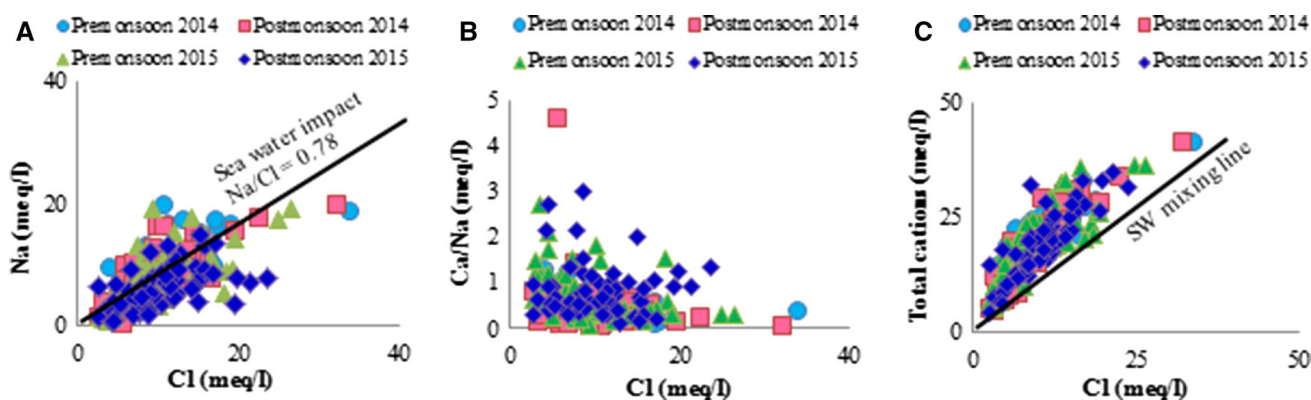


Fig. 13 Scatter plots of different ionic components a Na versus Cl, b Ca/Na versus Cl, c total cations versus Cl

Fig. 14 Map showing seasonal variation of seawater fraction and ionic deviation

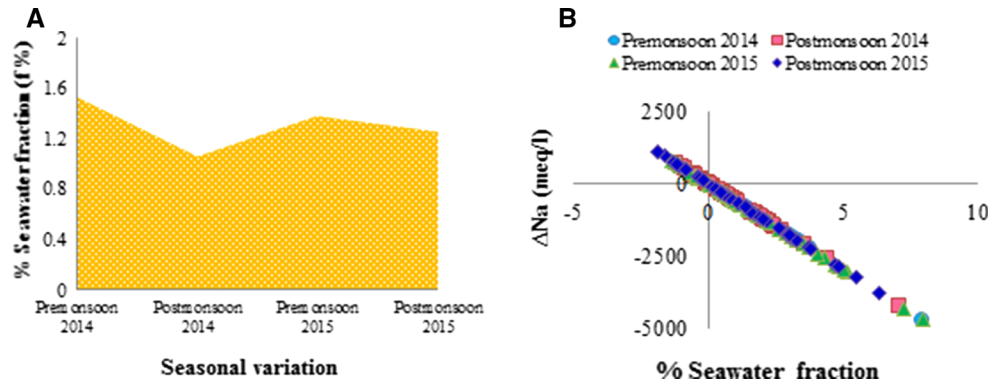
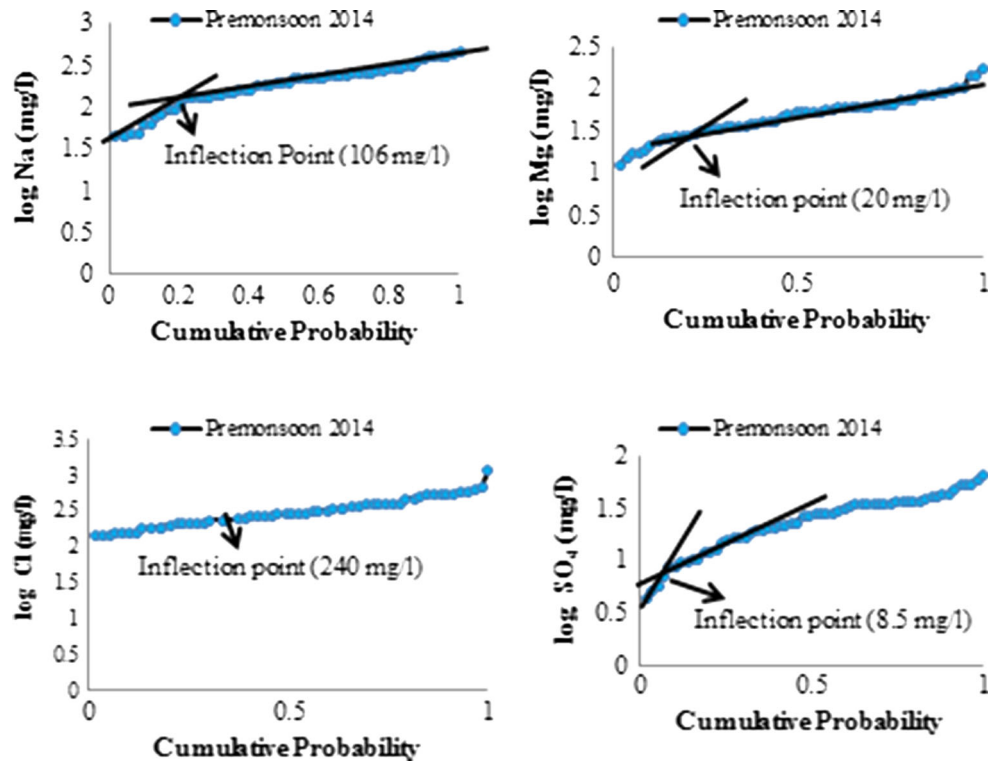


Fig. 15 Bivariate plot of cumulative probability versus log Na, Mg, Cl and SO₄



not affected by water–rock interactions (Vengosh and Pankratov 1998; Zghibi et al. 2014). Saline water encroachment can be evaluated by interpreting various bivariate ionic plots and ratios (Table 1). Na/Cl scatter diagram (Fig. 13a) and Na/Cl ratio <0.78 suggest the seawater intrusion in groundwater. Based on the Na/Cl ratio, around 34, 49, 45 and 50 % groundwater samples in pre- and post-monsoon of 2014 and 2015, respectively, indicate the seawater effect. However, these samples are also characterized by high concentration of NO₃, restricting the impact of seawater intrusion. These observations led to conclude that salinity source could be anthropogenic (constitutes Na, Cl and NO₃) as well as the influence from seawater intrusion (Voutsis et al. 2015).

Seawater is characterized by high Na, Mg, Cl and low Ca concentration, but freshwater has vice versa (Hem

1989). Lower Ca/Na ratio with high Cl indicates the seawater intrusion. In Ca/Na versus Cl plot, weak correlation indicates limited influence of seawater (Fig. 13b). However, few samples in studied seasons have high Cl with less Ca/Na demonstrating the seawater influence on hydrogeochemistry of the study area. Mg/Ca in freshwater is characterized between 0 and 1, and its value toward 5 indicates seawater influence (El Moujabber et al. 2006). According to this ratio distribution, around 67, 43, 69 and 50 % samples in pre- and post-monsoon of 2014 and 2015, respectively, are freshwater and only 3, 10, 2 and 3 % in pre- and post-monsoon of 2014 and 2015, respectively, constitute seawater influence. Thus, it is clear that majority of the sampling locations are not influenced by seawater intrusion or sea sprays, except few groundwater which are located nearby Bay of Bengal

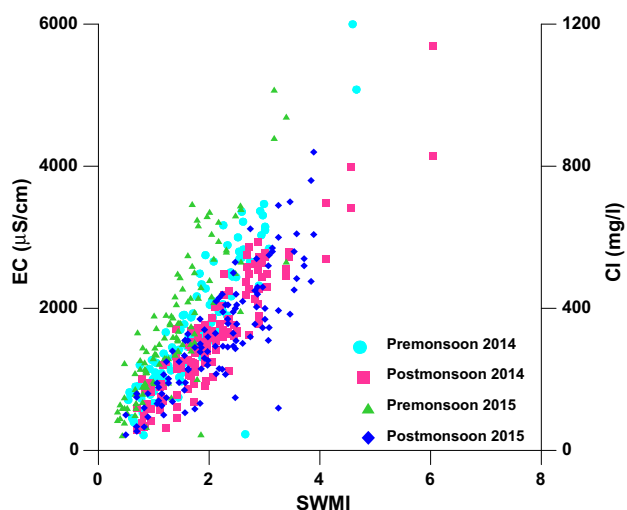


Fig. 16 Interrelationship between SWMI, EC and Cl

(Trabelsi et al. 2012; Arslan 2013). Todd (1959) classified the $\text{Cl}/(\text{HCO}_3 + \text{CO}_3)$ ratio for salinization as <0.5 indicates that groundwater is unaffected by saline water, $0.5\text{--}6.6$ for moderately affected and >6.6 for strong saline-affected groundwater. According to this classification, majority of the samples (90, 92, 93 and 95 % in pre- and post-monsoon of 2014 and 2015, respectively) fall in $0.5\text{--}6.6$ zone deducing that these groundwaters are moderately affected by saline water. Only few samples which are located nearby Bay of Bengal are strongly affected by saline water. To distinguish the different sources of Cl, i.e., saline water, irrigation runoff or wastewater, SO_4/Cl ratio is used and value toward higher side of 0.91 indicates seawater effect, while 0.14 reveals agricultural contamination (Jung et al. 2014). Average value of ratio is 0.12 in the studied seasons indicating the contribution of agricultural contamination such as excess fertilizer input or irrigation water runoff for Cl enrichment. In total cations versus Cl plot, majority of the data set showed upward deviation from seawater mixing line toward total cation due to mineral weathering which provides cation without effecting Cl in the groundwater (Fig. 13c). Few data points are also observed along the line suggesting seawater intrusion and high ion exchange between saltwater and clay fraction (Kim et al. 2004).

Saline water estimation in river basin

Results of $\%f_{\text{sea}}$ calculation are displayed in Table 1, and it is observed that the majority of values are positive indicating the presence of saltwater fraction (Fig. 14a). Some of the samples (sample nos. 19, 26, 27, 28) have higher $\%f_{\text{sea}}$ suggesting severe affect by saltwater of Bay of Bengal due to overextraction of coastal freshwater aquifers.

Few samples distant from coastal side have high value of f_{sea} indicating that the up-coning of paleobrine water beneath the freshwater may be due to over pumping of groundwater causing inland inversion of hydraulic gradient or agricultural contamination and wastewater infiltration.

Ionic deviation (Δ) of each ion is calculated and presented in Table 1. Most of the samples are showing high range of negative ΔNa and indicating the mixing of groundwater and sea/saline water which is further confirmed by high EC values. High ΔNa is proportional to $\%f_{\text{sea}}$ that can be explained as follows (Fig. 14b). In 2013, Phailin cyclone had developed in Bay of Bengal and appreciable amount of seawater encroached coastal regions. Likewise various cycles of cyclones, tsunamis along with periodical backwash water, form paleobrine water pockets in coastal areas, and further contact of groundwater with these pockets diffuses the saline constituents and results in brackish water. Direct contact of river with seawater could also increase the salinity of river water by cation exchange process and recharging nearby aquifers with saline river water. Generally, ΔCa and ΔHCO_3 values decrease with ΔMg and ΔSO_4 increment for seawater intrusion, but their disproportionate behavior limits the probability of seawater intrusion. Thus, it can be concluded that study area has restricted situation of saline/seawater intrusion with high impact in coastal areas by seawater and with high impact of anthropogenic sources (up-coning of saline or brine water due to over pumping of deep borewells, agricultural runoff and municipal, industrial wastewater) in mainland.

Sea/saline water mixing index (SWMI)

Cumulative probability curves and the log values of Na, Mg, Cl and SO_4 are interpreted to derive threshold value shown in Fig. 15. SWMI values >1.18 depict the probable interaction between saline water–fresh groundwater, whereas <1.18 with low EC and Cl concentration imparts the freshwater zone (Fig. 16). Higher SWMI values (>3) are found in sampling locations of 19, 26, 28, 34 which are close to the Bay of Bengal indicating the seawater intrusion, and locations 4, 9, 14, 45, 47, 49, 50, 52 and 53 in mainland indicate paleobrine presence, anthropogenic contamination or inverse hydraulic gradient due to heavy groundwater extraction in the coastal freshwater aquifers (Table 1). For well-defined identification, spatial distribution diagram of index has been plotted to demarcate the salinized zones of the basin (Fig. 17). In the diagram, high salinized zones mainly exist in coastal and urbanized areas indicating the seawater invasion and anthropogenic contaminant infiltration, respectively. These areas are also unevenly distributed with Na–Cl and Ca–Cl facies, as

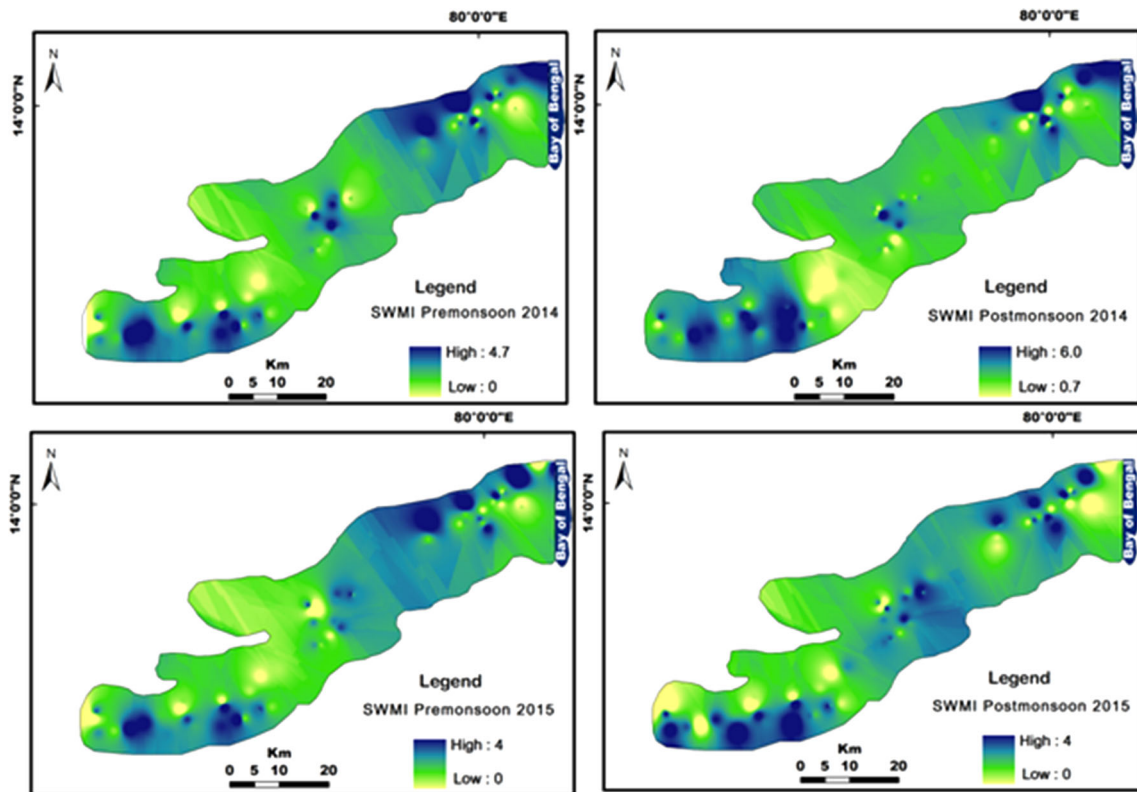


Fig. 17 Spatial distribution of calculated SWMI of Swarnamukhi river basin

shown by clusters of dendrogram supporting the salinization of the areas.

Conclusion

After interpretation of parameters by box–whisker plot, dominance of Na and HCO₃ in 2014 and Ca and HCO₃ in 2015 was observed. Logarithmic plot of Ca/Na versus HCO₃/Na suggests silicate followed by carbonate and evaporite weathering. Geochemical modeling reveals the undersaturation and saturation state of different minerals and prevalence of aluminosilicate minerals which on dissolution form kaolinite. WQI indicates excellent to good water for human utilization. Multivariate statistical tools suggest a mixed source of ions in groundwater. Salinity in coastal areas is due to seawater intrusion and anthropogenic activities in the mainland. Water–rock interactions, overexploitation of groundwater and heavy use of fertilizers and pesticides inputs are responsible for the spatio-temporal changes in the groundwater chemistry of the study area.

Acknowledgments The first author (NJR) is indebted to the University Grants Commission (UGC) for financial support under Major Research Project {(F. No. 42-413/2013 (SR))} and Jawaharlal Nehru University for providing UPOE II (ID 170) funds under holistic

development program. The authors are thankful to Mr. N. Amarnath Reddy and Dr. D. Shankar for their constant help and logistic support for sediment and water sample collection during field work of the project. Thanks are due to anonymous reviewers whose constructive suggestions/comments have improved the quality of manuscript.

References

Adams S, Titus R, Pietersen K, Tredoux G, Harris C (2001) Hydrochemical characteristics of aquifers near Sutherland in the Western Karoo, South Africa. *Hydrogeology* 241:91–103

APHA (2005) Standard methods for the examination of water and wastewater, 21st edn. American Public Health Association, Washington

Arslan H (2013) Application of multivariate statistical techniques in the assessment of groundwater quality in seawater intrusion area in Bafra Plain, Turkey. *Environ Monit Assess* 185:2439–2452

Ayeneu T, Demlie M, Wöhrlich S (2008) Hydrogeological framework and occurrence of groundwater in the Ethiopian aquifers. *J Afr Earth Sci* 52:97–113

Ball JW, Nordstrom DK (1991) WATEQ4F—user’s manual with revised thermodynamic database and test cases for calculating speciation of major, trace and redox elements in natural waters. United States Geological Survey, Open-File Report; 90–129

Bhardwaj V, Singh DS, Singh AK (2010) Hydrogeochemistry of groundwater and anthropogenic control over dolomitization reactions in alluvial sediments of the Deoria district: Ganga plain, India. *Environ Earth Sci* 59:1099–1109

Cendón DI, Ayora C, Pueyo JJ, Taberner C, Blanc-Valleron MM (2008) The chemical and hydrological evolution of the Mulhouse potash basin (France): are “marine” ancient evaporites

- always representative of synchronous seawater chemistry? *Chem Geol* 252:109–124
- Devic G, Djordjevic D, Sakan S (2014) Natural and anthropogenic factors affecting the groundwater quality in Serbia. *Sci Total Environ* 468–469:933–942
- Einsiedl F (2012) Sea-water/groundwater interactions along a small catchment of the European Atlantic coast. *Appl Geochem* 27:73–80
- El Moujabber M, Bou SB, Darwish T, Atallah T (2006) Comparison of different indicators for groundwater contamination by seawater intrusion on the Lebanese coast. *Water Resour Manag* 20:161–180
- Fidelibus MD (2003) Environmental tracing in coastal aquifers: old problems and new solutions. In: *Aquifers Coastal (ed) Intrusion technology: Mediterranean countries, vol II*. Publ. IGME, Madrid, pp 79–111
- Gaillardet J, Dupre B, Louvat P, Allègre CJ (1999) Global silicate weathering and CO₂ consumption rates deduced from the chemistry of large rivers. *Chem Geol* 159:3–30
- Gueroui Y, Maoui A, Touati AS (2014) Hydrochemical and bacteriological investigation in groundwater of the Tamlouka Plain, north-east of Algeria. *Arab J Geosci* 8:2417–2432
- Helgeson HC (1968) Evaluation of irreversible reactions in geochemical processes involving minerals and aqueous solutions—I thermodynamic relations. *Geochim Cosmochim Acta* 32:853–877
- Hem JD (1989) Study and interpretation of the chemical characteristics of natural water. USGS water supply paper 2254. US Government Printing Office, Washington
- Herojeet RK, Rishi MS, Sidhu N (2013) Hydrochemical characterization, classification and evaluation of groundwater regime in Sirsa Watershed, Nalagarh Valley, Himachal Pradesh, India. *Civil Environ Res* 3:47–57
- Jankowski J, Acworth RI (1997) Impact of debris-flow deposits on hydrogeochemical processes and the development of dryland salinity in the Yass River Catchment, New South Wales, Australia. *Hydrogeology* 5:71–88
- Jiang Y, Wu Y, Groves C, Yuan D, Kambesis P (2009) Natural and anthropogenic factors affecting the groundwater quality in the Nandong karst underground river system in Yunan, China. *J Contam Hydrol* 109:49–61
- Jung HW, Yun ST, Kim KH, Oh SS, Kang KG (2014) Role of an impermeable layer in controlling groundwater chemistry in a basaltic aquifer beneath an agricultural field, Jeju Island, South Korea. *Appl Geochem* 45:82–93
- Junior RFV, Varandas SGP, Fernandes LFS, Pacheco FAL (2014) Groundwater quality in rural watersheds with environmental land use conflicts. *Sci Total Environ* 493:812–827
- Kim K, Rajmohan N, Kim HJ, Hwang GS, Cho MJ (2004) Assessment of groundwater chemistry in a coastal region (Kunsan, Korea) having complex contaminant sources: a stoichiometric approach. *Environ Geol* 46:763–774
- Kumar SK, Bharani R, Magesh NS, Godson PS, Chandrasekar N (2014) Hydrogeochemistry and groundwater quality appraisal of part of south Chennai coastal aquifers, Tamil Nadu, India using WQI and fuzzy logic method. *Appl Water Sci* 4:341–350
- Lepeltier C (1969) A simplified statistical treatment of geochemical data by graphical representation. *Econ Geol* 64:538–550
- Machiwal D, Jha MK (2015) Identifying sources of groundwater contamination in a hard-rock aquifer system using multivariate statistical analyses and GIS-based geostatistical modeling techniques. *J Hydrol Reg Stud* 4:80–110
- Majumder RK, Hasnat MA, Hossain S, Ikeue K, Machida M (2008) An exploration of nitrate concentrations in groundwater aquifers of central-west region of Bangladesh. *J Hazard Mater* 159:536–543
- Molina-Navarro E, Sastre-Merlín A, Vicente R, Martínez-Pérez S (2014) Hydrogeology and hydrogeochemistry at a site of strategic importance: the Pareja Limno-reservoir drainage basin (Guadalajara, central Spain). *Hydrogeology* 22:1115–1129
- Mondal NC, Singh VP, Singh S, Singh VS (2011) Hydrochemical characteristic of coastal aquifer from Tuticorin, Tamil Nadu, India. *Environ Monit Assess* 175:531–550
- Montcoudiol N, Molson J, Lemieux JM (2014) Groundwater geochemistry of the Outaouais Region (Québec, Canada): a regional-scale study. *Hydrogeology* 23:377–396
- Nampak H, Pradhan B, Manap MA (2014) Application of GIS based data driven evidential belief function model to predict groundwater potential zonation. *J Hydrol* 513:283–300
- Njitchoua R, Dever L, Fontes JCH, Naah E (1997) Geochemistry, origin and recharge mechanisms of groundwater from the Garoua Sandstone aquifer, northern Cameroon. *J Hydrol* 190:123–140
- Okiongbo KS, Douglas RK (2014) Evaluation of major factors influencing the geochemistry of groundwater using graphical and multivariate statistical methods in Yenagoa city, Southern Nigeria. *Appl Water Sci* 5:27–37
- Park S, Yun S, Chae G, Yoo I, Shin K, Heo C, Lee S (2005) Regional hydrochemical study on salinization of coastal aquifers, western coastal area of South Korea. *J Hydrol* 313:182–194
- Rajmohan N, Elango L (2004) Identification and evolution of hydrogeochemical processes in the groundwater environment in an area of the Palar and Cheyyar River Basins, Southern India. *Environ Geol* 46:47–61
- Raju NJ (2012) Evaluation of hydrogeochemical processes in the pleistocene aquifers of middle Ganga plain, Uttar Pradesh, India. *Environ Earth Sci* 65:1291–1308
- Raju NJ, Reddy TVK (1998) Fracture pattern and electrical resistivity studies for groundwater exploration. *Environ Geol* 34:175–182
- Raju NJ, Reddy TVK (2007) Environmental and urbanization affect on groundwater resources in a pilgrim town of Tirupati, Andhra Pradesh, South India. *J Appl Geochem* 9:212–223
- Raju NJ, Reddy TVK, Nayudu PT (1996) Electrical resistivity surveys for groundwater in the upper Gunjanaeru catchment, Cuddapah district, Andhra Pradesh. *J Geol Soc India* 47:705–716
- Raju NJ, Ram P, Dey S (2009) Groundwater quality in the lower Varuna River basin, Varanasi district, Uttar Pradesh. *J Geol Soc India* 73:178–192
- Raju NJ, Shukla UK, Ram P (2011) Hydrogeochemistry for the assessment of groundwater quality in Varanasi: a fast-urbanizing center in Uttar Pradesh, India. *Environ Monit Assess* 173:279–300
- Raju NJ, Dey S, Gossel W, Wycisk P (2012) Fluoride hazard and assessment of groundwater quality in the semi-arid Upper Panda River basin, Sonbhadra district, Uttar Pradesh, India. *Hydrol Sci* 57:1433–1452
- Raju NJ, Reddy TVK, Muniratnam P, Gossel W, Wycisk P (2013) Managed aquifer recharge (MAR) by the construction of subsurface dams in the semi-arid regions: a case study of the Kalangi River basin, Andhra Pradesh, India. *J Geol Soc India* 82:657–665
- Rao GT, Rao VVSG, Rao YS, Ramesh G (2013) Study of hydrogeochemical processes of the groundwater in Ghatprabha river sub-basin, Bagalkot district, Karnataka, India. *Arab J Geosci* 6:2447–2459
- Rasouli F, Pouya AK, Cheraghi SAM (2012) Hydrogeochemistry and water quality assessment of the Kor–Sivand Basin, Fars province, Iran. *Environ Monit Assess* 184:4861–4877
- Reddy CV, Kotaiah B, Raju NJ (1992) A study on groundwater quality near a municipal solid waste disposal site at Tirupati, Andhra Pradesh, India. *Fresenius Environ Bull* 1:93–97

- Reddy MR, Raju NJ, Reddy YV, Reddy TVK (2000) Water resources development and management in the Cuddapah district, Andhra Pradesh, India. *Environ Geol* 39:342–352
- Salman A, Al-Qinna M, Al Kuisi M (2014) Spatial analysis of soil and shallow groundwater physicochemical parameters in El-Mujib Basin-central Jordan. *J Asian Earth Sci* 79:366–381
- Sawyer CN, McCarty PL, Parkin GF (1994) *Chemistry for environmental engineering, civil engineering series*, 4th edn. New Delhi, McGraw-Hill
- Semhi K, Amiotte Suchet P, Clauer N, Probst J-L (2000) Impact of nitrogen fertilizers on the natural weathering–erosion processes and fluvial transport in the Garonne basin. *Appl Geochem* 15:865–874
- Shiklomanov IA (1993) World fresh water resources. In: Gleick PH (ed) *Water in crisis: a guide to world's fresh water resources*. Oxford University Press, New York
- Sinclair AJ (1974) Selection of thresholds in geochemical data using probability graphs. *J Geochem Explor* 3:129–149
- Singh S, Raju NJ, Ramakrishna Ch (2015) Evaluation of groundwater quality and its suitability for domestic and irrigation use in parts of the Chandauli–Varanasi region, Uttar Pradesh, India. *J Water Resour Prot* 7:482–497
- Stumm W, Morgan JJ (1996) *Aquatic chemistry: chemical equilibria and rates in natural waters*, 3rd edn. New York, Wiley, p 1022
- Svetlana V, Kolakovic S, Masic B (2012) Application of chemometric technique in the assessment of water quality of Tisza River (Serbia). *Adv Res Sci Areas* 3–7:1595–1601
- Taylor SR, McLennan SM (1985) *The continental crust: its composition and evolution*. Blackwell, London, p 312
- Todd DK (1959) *Ground water hydrology*. Wiley, New York
- Toumi N, Hussein BH, Rafrafi S, El Kassas N (2015) Groundwater quality and hydrochemical properties of Al-Ula Region, Saudi Arabia. *Environ Monit Assess* 187:1–16
- Trabelsi R, Abid K, Zouari K, Yahyaoui H (2012) Groundwater salinization processes in shallow coastal aquifer of Djefara plain of Medenine, Southeastern Tunisia. *Environ Earth Sci* 66:641–653
- Vengosh A, Pankratov I (1998) Chloride/bromide and chloride/fluoride ratios of domestic sewage effluents and associated contaminated ground water. *Ground Water* 36:815–824
- Voutsis N, Kelepertzis E, Tziritis E, Kelepertzis A (2015) Assessing the hydrogeochemistry of groundwaters in ophiolite areas of Euboea Island, Greece, using multivariate statistical methods. *J Geochem Explor* 159:79–92
- WHO (1997) *Guidelines for drinking water quality, health criteria and other supporting information*, 2nd edn. WHO, Geneva, pp 940–949
- WHO (2006) *Guidelines for drinking water quality. Incorporating first addendum, recommendations*, 3rd edn. World Health Organization, Geneva, p 515
- Zghibi A, Merzougui A, Zouhri L, Tarhouni J (2014) Understanding groundwater chemistry using multivariate statistics techniques to the study of contamination in the Korba unconfined aquifer system of Cap-Bon (North-east of Tunisia). *J Afr Earth Sci* 89:1–15
- Zhang B, Song X, Zhang Y, Han D, Tang C, Yu Y, Ma Y (2012) Hydrochemical characteristics and water quality assessment of surface water and groundwater in Songnen plain, Northeast China. *Water Res* 46:2737–2748
- Zhu D, Ryan MC, Sun B, Li C (2014) The influence of irrigation and Wuliangshuai Lake on groundwater quality in eastern Hetao Basin, Inner Mongolia, China. *Hydrogeology* 22:1101–1114
- Zouahri A, Dakak H, Douaik A, El Khadir M, Moussadek R (2014) Evaluation of groundwater suitability for irrigation in the Skhirat region, Northwest of Morocco. *Environ Monit Assess* 187:4184